NATIONAL AERONAUTICS AND SPACE ADMINISTRATION

TECHNICAL MEMORANDUM X-799

AN APPROACH TO OBTAINING INCREASED SUPERSONIC LIFT-DRAG RATIOS AND REDUCED SONIC BOOM*

By Richard T. Whitcomb

ABSTRACT

Several means for improving the lift-drag ratios of configurations with arrow wings swept behind the Mach angle are described. The most important of these factors is the integration of the engine nacelles into the rearward part of the wing. Experimental results for a representative wing-fuselage-nacelle combination based on the proposed approach indicate reduced sonic boom, as well as improved lift-drag ratios.

I

NATIONAL AERONAUTICS AND SPACE ADMINISTRATION

TECHNICAL MEMORANDUM X-799

AN APPROACH TO OBTAINING INCREASED SUPERSONIC LIFT-DRAG RATIOS AND REDUCED SONIC BOOM*

By Richard T. Whitcomb

SUMMARY

Several means for obtaining improved characteristics for airplane combinations incorporating arrow wings swept behind the Mach angle are suggested. In the several parts of the overall approach, a small ratio of wing root chord to wing length is used to improve the drag due to lift, the engine nacelles are integrated into the rearward part of the wing to reduce the adverse thickness effects, the fuselage is cambered to reduce the trim drag, and a wing leading-edge sweep approaching the Mach angle is utilized to allow improvements of the off-design performance. Selected experimental results for a representative wing-fuselage-nacelle combination designed for a maximum Mach number of 3.2 on the basis of the proposed approach are presented to provide an indication of the effectiveness of the various included factors. Experimental results are also presented which indicate that a configuration based on the proposed approach should produce a substantially lower sonic-boom overpressure than would be obtained for a comparable delta-wing combination.

INTRODUCTION

It is generally agreed that the attainment of a competitive long-range supersonic commercial aircraft requires, among other factors, the achievement of supersonic lift-drag ratios substantially higher than those obtainable with a simple delta-wing configuration. Further, to provide acceptable sonic-boom levels at the ground with a reasonable climb-acceleration flight path for such an airplane will require boom overpressures substantially lower than those for aircraft presently operating. (See ref. 1.) A number of methods for accomplishing these objectives are now being studied. One approach, a special treatment of a highly swept arrow wing, is described herein.

Linear-theory analyses indicate that supersonic lift-drag ratios significantly greater than those for the delta-wing configuration might be obtained through the use of a cambered arrow wing having a leading edge swept behind the Mach angle and a trailing edge with substantial sweepback. (See refs. 2 and 3.)

Theory also indicates that the highly swept arrow wing should result in a relatively low sonic-boom overpressure. Because of the theoretical promise of the arrow wing, a number of experimental studies have been made of such configurations. (See refs. 4 to 7, for example.) These investigations indicate lift-drag ratios substantially less than the predicted values. The disappointing lift-drag ratios for these wings result from actual drag-due-to-lift factors substantially greater than those predicted by theory. As pointed out in reference 3, these differences are primarily a consequence of strong distortions of the actual flow fields from those assumed in the theory. (In this report these distortions will be referred to as nonlinear effects.)

In the present design approach, the lift-drag ratios for a highly swept wing airplane configuration are improved by shaping and arranging the various components to reduce the lift-induced drag below that previously achieved and to lessen the drag due to thickness. Means are also provided to reduce the drag penalty associated with providing trim pitching moments and to improve the off-design characteristics. The basic considerations of this proposed method, together with selected experimental results for a representative wing-fuselage-nacelle configuration designed on the basis of the approach, are described and discussed herein. Results of investigations of an airplane configuration based on the approach for the range of probable flight conditions are presented in references 8 and 9.

SYMBOLS

b	span of wing, ft
c	local chord of wing, in.
$\bar{c}$	mean chord of wing, ft
C_D	drag coefficient
c_l	local section lift coefficient
c_r	root chord, in.
C_L	lift coefficient
C_m	pitching-moment coefficient
C_p	pressure coefficient, $\frac{p_{local} - p_\infty}{q}$
i	incidence of a wing section, deg
l	longitudinal length of wing from apex to tip

L characteristic length of sonic-boom model (1.15 inches for present investigation)

M Mach number

m maximum displacement of mean line of a wing section from a straight line from leading edge to trailing edge, in.

p free-stream static pressure, lb/sq ft

Δp_{max} maximum incremental pressure at bow shock due to flow field of sonic-boom model, lb/sq ft

q free-stream dynamic pressure, lb/sq ft

S reference wing area, sq ft

t thickness of wing section, in.

V volume of configuration, cu ft

x, z Cartesian coordinates of airfoil sections, x in chordwise direction

x' distance from leading edge of a wing section, in.

y lateral distance, in.

α angle of attack, referred to top of rear part of fuselage, deg

$\beta = \sqrt{M^2 - 1}$

θ rotation from the upward vertical of the oblique cutting planes for obtaining cross-sectional areas

Λ wing leading-edge sweep angle, deg

Subscripts:

l lower surface

u upper surface

∞ conditions of undisturbed stream

w wave

BASIC CONSIDERATIONS

Drag Due to Lift

Linear theory analysis (ref. 3) indicates that the drag-due-to-lift factor can be substantially decreased by reducing the ratio of wing root chord to wing length c_r/l. Also, an analysis of the probable local flow near the wing suggests that such a change should not result in a significant increase of the adverse deviation of the actual factor from the theoretical values. Therefore, in the present approach an attempt has been made to achieve a drag due to lift below the level established for the best cambered and twisted arrow wings previously investigated (refs. 5 and 6) by using a smaller ratio of root chord to length than was incorporated in those wings.

Exploratory investigations of various twist and camber distributions on the configuration of the present approach have disclosed no shape which allows a significantly closer approach to the theoretical optimum than that provided by the best previous configurations at least for values of $\beta \cot \Lambda$ similar to the design values of those wings.

Drag Due to Thickness

To provide a reasonable strength-weight ratio for a highly swept arrow wing with a low ratio of root chord to length, as proposed for the present approach, the section thickness ratios must be made relatively large. For the usual wing-fuselage combination, this requirement results in a high minimum wave drag. Analysis and unpublished experiments indicate that such increased thickness ratios also result in significantly greater deviations of the actual drag due to lift from the theoretical optimum. This adverse effect probably results primarily from an aggravation of the nonlinear distortions of the flow fields by the induced flows associated with thickness. One of the primary objectives of the present approach has been to reduce these several thickness effects.

An analysis of the zero-lift pressure distributions on highly swept arrow wings indicates that most of the pressure drag for such configurations is associated with severe negative pressures along the aft portions of the midspans and outboard streamwise wing sections, at least for values of $\beta \cot \Lambda \approx 0.8$. (For example, see fig. 1 based on data from ref. 10.) Divergence of the upper and lower surface elements of the sections in this region should substantially reduce the drag. Such a change lessens the local negative pressure and, more importantly, reduces the drag component of the remaining pressure decrement. However, such a divergence of the wing elements would obviously result in a base area with a large drag increment. An effect similar to that of diverging wing elements is provided by placing bodies similar to those of reference 11 along the aft portion of the wing. As suggested in reference 12, these bodies may be used to house the engines.

To provide a significant reduction of drag, the elements of these added bodies should have substantial streamwise divergence along the aft portion of

the wing. Part of the desired divergence is provided by the longitudinal increase of cross-sectional area of the nacelles required to meet to the engine air-flow requirements of the higher supersonic Mach numbers. The divergence in the critical region may be increased by locating the inlets so that the part of the air-induction system requiring the minimum stream tube area is located near the maximum thickness of the wing. With such an arrangement, the net added cross-sectional area of the nacelle in the region of the maximum wing thickness may be made substantially less than the inlet area. The effective surface divergence provided by the nacelles may be further increased for a configuration with a large trailing-edge sweep by providing a "toe-in" of the nacelle along the aft portion of the wing. Such an arrangement provides a desired increase of divergence of the outer elements of the nacelle which are directly adjacent to the aft portion of the wing. (See fig. 2.) Of course, the toe-ins also result in a decrease of the divergence of the inboard sides of the nacelles. However, this adverse change is well removed from the critical region; thus, its effect is far less than that of the favorable divergence of the outer surfaces.

The effective wing section shapes provided by the proposed nacelle addition, for the configuration of figure 2, as determined by the area-rule procedure described in appendix A are shown in figure 3. (The discontinuities of these effective shapes near the leading edge of the lower surface of the midsemispan sections result from the area buildup of the inlets in these regions.) The favorable effect of the suggested nacelle arrangement on the longitudinal developments of cross-sectional area (appendix A) for the configuration of figure 2 at a Mach number of 3.2 are shown in figure 4.

The proposed placement of the nacelles should also reduce the effect of thickness on the drag due to lift, as noted previously, compared with that for a wing-fuselage combination. In addition, it should result in a skin-friction drag increment substantially less than that for comparable pylon-mounted nacelles.

Analysis of surface pressures and longitudinal area developments (appendix A) indicate that the zero-lift drag for a highly swept wing can be further reduced by extending the longitudinal coordinates of the root section rearward as shown in figure 2. Such a modification also allows a significant reduction of the structural weight for wing sections near the fuselage since it allows a rearward shift of the main structural members in this region.

Area-rule analyses and exploratory experiments indicate little improvement in the zero-lift pressure drag is gained by shaping the fuselage beyond that obtained through the use of an approximately uniform cross-sectional area in the region of the wing root with roughly conical area developments forward and rearward of that region. Obviously, for minimum drag the cross-sectional area of the fuselage in the region of the wing root should be as small as practical.

Trimming Moment

The positive zero-lift pitching moment required to provide cruise trim at supersonic speeds is usually large if the airplane center of gravity is located to allow adequate stability at subsonic speeds. Results obtained for highly

swept arrow wings alone (ref. 6) suggest that the camber and twist required to obtain low drag due to lift should produce a substantial part of this required trimming moment for complete configurations. Providing the additional necessary moment by a forward or aft tail load may result in a significant drag penalty. Producing the moment by an increase in the incidence of the fuselage ahead of the wing (ref. 13) can cause drag and stability problems, particularly at off-design conditions. Forebody incidence also severely increases the problem of obtaining adequate pilot visibility. Exploratory experiments indicate that providing the required moment by additional washout of the wing tip may result in an excess increase in drag due to lift. The adverse effect of such a change would be quite pronounced for a relatively flexible actual airplane configuration.

Analyses and exploratory experiments for the proposed configuration indicate that the added moment can be obtained with very little drag penalty by increasing the lift on the forward parts of the wing and on the fuselage near the forward region of the wing-fuselage juncture beyond that required for the lowest possible drag due to lift without regard to providing trim. Such a change in the load distribution results in a significant increase of the adverse pressure gradients on the inboard region of the upper surface of the wing with an increased possibility of boundary-layer separation in this region. The severity of such an increase in the gradients is substantially reduced by producing the required lift primarily with an increase of the incidence of the fuselage along the forward region of wing-fuselage juncture rather than by increasing the local slopes of the wing. A similar fuselage change on a subsonic configuration (ref. 14) provided a substantial increase in the pitching moment with no apparent adverse effect on the boundary-layer flow on the wing.

Off-Design Conditions

Induced-drag and low-speed characteristics.- The lift-drag ratios at speeds less than the design value and the landing and take-off performance for a fixed highly swept arrow-wing configuration are obviously limited because of the relatively low aspect ratio for such a configuration. In the present approach the inherent off-design performance capability has been increased by providing the highest possible aspect ratio compatible with achieving high design lift-drag ratios and providing a reasonable structure. The aspect ratio is, of course, increased by the use of a low ratio of root chord to length, as proposed, to improve the design performance.

Available information suggests that the aspect ratio can also be increased without a significant penalty in high-speed performance by using a leading-edge sweep angle which is relatively close to the Mach angle for the design condition, that is, for $\beta \cot \Lambda$ approaching 1.0. Linear theory indicates that such an approach leads to significant increases in both the minimum drag (ref. 15) and the drag due to lift. (See fig. 5.) However, it may be assumed that, with the special placement of the engine nacelles, the actual increase in minimum drag should be small to relatively high values of $\beta \cot \Lambda$. Further, because of reductions of the nonlinear effects with an increase in $\beta \cot \Lambda$, the increase of the actual drag due to lift should be substantially less than that predicted by theory.

This decrease of the nonlinear effects with an increase in $\beta \cot \Lambda$ results from a marked decrease of the maximum induced pressures on the upper surface of the critical forward portion of the outboard sections required to obtain load distributions indicated as optimum by linear theory. (See ref. 3.) The estimated change for the 0.7-semispan station of a wing with a ratio $\frac{c_r}{l} = 0.55$, and a 5-percent-thick circular-arc airfoil at a Mach number of 3.2 and a lift coefficient of 0.075 is shown in figure 5(b). Part of this variation results from a reduction of the local load needed for minimum drag. Such a decrease is predicted by linear theory (ref. 3) and it may be assumed that the actual required loads vary similarly. (The theoretical variations were used in the analysis of fig. 5(b).)

Most of the change of the upper-surface induced pressures with $\beta \cot \Lambda$ is associated with a substantial increase of the positive pressures on the lower surface. Obviously, with such a change the upper-surface pressures required to obtain a given local load are reduced. The actual pressure coefficients near the leading edge of the lower surface and the variation of these pressures with $\beta \cot \Lambda$ are substantially different than those predicted by linear theory. (See fig. 5(c) based on results from ref. 10 and also ref. 16.) These deviations result primarily from the fact that the pressures in this region of an arrow wing approach limiting values corresponding to the achievement of a stagnation condition for the Mach number component normal to the leading edge. (See fig. 5(c).) In the present analysis, this limiting pressure coefficient was approximated by the relationship:

$$C_p = \cos^2\Lambda(1 + 0.25M^2\cos^2\Lambda)$$

which is based on simple infinite-span sweep theory and one-dimensional flow relationships. It is apparent from this expression that this limiting pressure value increases rapidly with a decrease of sweep angle.

Boundary-layer separation.- The surface oil-flow surveys of references 5, 6, and 17 indicate that substantial flow separation develops on the upper surface of highly swept wings at lift coefficients just above those for maximum lift-drag ratios for all Mach numbers up to the design condition. This separation results in increases in drag and adverse changes of the stability characteristics. In the proposed approach, the portions of nacelles above the upper surface of the wing should reduce this boundary-layer separation as did the bodies of reference 11. The separation at off-design conditions is also reduced by use of a rounded-wing leading edge and the greatest camber possible compatible with obtaining high lift-drag ratios at the design condition.

Sonic Boom

To reduce the sonic boom at the ground, supersonic cruise airplanes will probably operate at high altitudes during the various supersonic phases of the flight. For the high lift coefficients associated with such operations, the boom due to lift will be of the same order as that resulting from volume. (See

ref. 1.) Therefore, in any attempt to reduce the magnitude of the boom overpressure, the problem at lifting conditions should be considered.

Linear theory analysis, such as presented in reference 18, provides a reasonably close approximation of the sonic-boom overpressure for the usual delta-wing supersonic airplane configuration at lifting conditions. (See ref. 19.) This theory would appear, therefore, to be a reasonably satisfactory approach for evaluating means for reducing the magnitude of the boom. The method indicates that the boom level at high lift coefficients for an airplane configuration having a highly swept arrow wing with a large cutout, such as the proposed combination, should approach the theoretical minimum level. (See ref. 20.)

An arrow wing swept behind the Mach angle should provide important reductions in the boom overpressure in addition to that predicted by linear theory. As indicated in figure 5, the proportion of the total lift carried by the lower surface of the wing is substantially less than that predicted by theory. Since the boom is caused primarily by the effects produced by the lower part of the configuration, it might be expected that this reduced lower surface lift would result in an actual boom less than that predicted by theory.

Area rule analyses (appendix A) indicate that at supersonic speeds the longitudinal buildup of the positive disturbances produced by the forward part of the wing is significantly extended and reduced by wing dihedral. Thus, it might be expected that this factor would result in a reduction in boom intensity.

The placement of the engine nacelles relatively far rearward with respect to the maximum cross-sectional area for the wing fuselage, as in the presently proposed approach, allows a significant reduction of the maximum total cross-sectional area with a resulting lessening of the boom overpressure.

EXPERIMENTS

Configurations

The representative wing-fuselage-nacelle combination developed to demonstrate the effectiveness of the proposed approach is shown in figures 2(a) to 2(c). Photographs of a complete airplane configuration incorporating the various concepts are shown in figure 2(d). The configuration has been designed to provide high lift-drag ratios for flight Reynolds numbers at Mach numbers to about 3.2. In shaping the various components, consideration has been given to providing for satisfactory structural and operational characteristics as well as to obtain improved supersonic performance.

Wing.- Pertinent dimensional parameters of the wing are shown in figure 2(a) and table I; cross-sectional shapes are illustrated in figure 2(b); and spanwise variations of the thickness, camber, and twist are presented in figure 2(c). With the 74.5° of leading-edge sweep utilized, the parameter $\beta \cot \Lambda$ is about 0.84 for the maximum Mach number of 3.2.

With the wing planform used, the most critical bending moments would probably occur near the inboard side of the inner nacelles. Therefore, the sections in this region have been made particularly thick (5.5 percent at the 0.35 semispan station). With the thickness utilized, the ratio of the span of the panel outboard of the critical region to the local maximum thickness is about 26. The comparable ratio for the wing-fuselage juncture is the same. A brief analysis of the possible flutter characteristics and bending loads for an actual airplane wing based on the experimental configuration is presented in appendix B.

The camber and twist distributions for the representative combination shown in figures 2(c) and 3 were arrived at on the basis of extensive force and pressure distribution experiments. In this development, an attempt was made to approximate the pressure distributions shown in figure 6 at Mach numbers near 3.0. Linear theory analyses, together with comparisons of the experimental results of references 5, 6, 10, and 16, and considerations of the probable nonlinear effects suggest that such distributions should result in drag-due-to-lift values at least approaching the minimum and also provide the required zero-lift pitching moment for trim. The shapes referred to as "basic" in figure 2 were designed to approach these distributions closely. Those referred to as "leading edge drooped" incorporate increases in the twist and camber of the forward region of the out-board wing sections. This modification of the wing design was intended to reduce the boundary-layer separation on the outboard section of the basic configuration, indicated by surface oil-flow surveys (fig. 7), and to improve the low-speed characteristics. These modifications were accomplished by a lowering of the leading edge which varied linearly from 0 at the wing-fuselage juncture to 0.07 inch at the tip.

In general, the magnitudes of effective cambers of the various sections of the proposed configuration (figs. 3 and 2(c)), even for the model with added leading-edge droop, are substantially less than those for the cambered swept wings of references 5 to 7. The magnitude of the overall twist for the basic configuration is also significantly less. (See fig. 2.) However, with the leading edge drooped, the magnitude of twist is roughly similar to that for the wing of reference 5 designed for $C_L = 0.08$ and the wing of reference 6. It should be emphasized that the actual aerodynamic twist of the various models was substantially greater than these built-in twists because of aeroelastic deflections. Measurements made during the investigation of the present configuration indicate that such deflections increased the washout at the tip by about 0.3° for a lift coefficient of 0.12 at a Mach number of 2.9. For an actual airplane, the twist due to load at cruise conditions would probably be substantially greater than this value.

Except for the rounded leading edge, the thickness distributions for the wing sections approximate those of circular-arc airfoils. The leading-edge radius is 0.05 inch for all sections from root to tip.

The low-wing arrangement allows the wing structure to pass below the fuselage compartment and permits a landing gear of minimum length, as for the usual subsonic transport. The dihedral utilized provides adequate ground clearance for the outboard nacelle at the probable landing attitude.

Nacelles and inlets.- The arrangement of the nacelle shown should allow the placement of the engines behind the main wing structure with the ducting of the engine air below this beam. The nacelles have been sized to simulate those required for fan-type engines.

The engine air inlets incorporated in the configuration would provide internal compression in a manner similar to that for the two-dimensional inlets of reference 21. The particular inlet orientation used allows the minimum internal flow area to be located near the maximum wing thickness as desired. Also, with this arrangement the boundary-layer travel ahead of the inlet is probably sufficiently small to eliminate the need for the usual boundary-layer bypass. The inlet "toe-in" utilized provides approximate alinement of the vertical sides of the inlet with local flow at the supersonic cruise condition. The reduced depth of the inboard sides of the inlets, together with burying part of this depth below the wing contours, should result in a reduction of the possible adverse effects of large crossflows on the flow along the inner sides of the nacelles at off-design conditions. The surface oil flows of figure 7 indicate that inlets have only slight effects on the boundary-layer flow on the wing at near-design conditions. (In order to provide a duct flow in the model which would allow satisfactory internal drag determinations, it was necessary to make the size of the inlets roughly 20 percent smaller than that which would probably be needed for an actual airplane.)

To accentuate the favorable effect of the nacelles on the upper-surface boundary-layer separation at off-design condition, as discussed earlier, major parts of the rearward portions of the nacelles have been located above the wing for the combination investigated, even though such a procedure might result in an aggravation of the internal ducting problems. However, the exceptionally good off-design characteristics obtained for this configuration even at extreme conditions (ref. 8) suggest that satisfactory off-design stability can probably be achieved with the nacelles placed substantially lower with respect to the wing than the positions used for the test configuration. Of course, with such a change the wing trailing edge in the regions of the nacelles should be raised to provide the same equivalent section shapes as those shown in figure 3.

Analysis and exploratory experiments indicate the 4° toe-in of the portions of the nacelles under the wing and 0° above as shown in figure 2 are probably reasonably close to the optimum angles for a Mach number of 3.0 and a lift coefficient of 0.08. This difference between the angles below and above the wing results from the crossflows near the wing at lifting conditions.

Fuselage.- The maximum frontal area of the fuselage is about 2.3 percent of the wing area. With this fuselage size, the volume factor $\frac{V^{2/3}}{S}$ for the total configuration is roughly 0.178. In determining this value the volume of the stream tubes of air through the inlets has been subtracted from the total.

As indicated by the results of reference 14, the longitudinal location of the corner initiating the increased fuselage slope in the vicinity of the forward part of the wing-fuselage juncture is fairly critical. An excessively rearward location results in an adverse change in the flow field with an increase in wave

drag. A large forward displacement results in excessive upflow which may cause boundary-layer separation near the wing leading edge. Area-rule analyses and results presented in reference 8 suggest that a location somewhat forward of that for the present experimental configuration (fig. 2) should provide a somewhat lower drag at the design condition than that obtained with the location utilized herein.

Methods

Force investigation.- The selected aerodynamic characteristics presented herein have been obtained in the Langley Unitary Plan wind tunnel at a Reynolds number of 3×10^6 (based on the mean aerodynamic chord). Details of the procedures used are described in reference 8. To assure a turbulent boundary layer, a strip of No. 120 carborundum was placed just rearward of the leading edges of the wing and a strip of No. 80 carborundum was located near the fuselage nose. The results presented have been corrected for the internal drag in the nacelles. (See ref. 8.) As pointed out in reference 8, these corrections include the energy loss of the boundary layer of the wing ahead of inlet ingested into the internal system. Because of this effect, these drag-coefficient corrections are probably about 0.0001 greater than the actual internal drag.

In addition to investigations of the complete configuration with and without leading-edge droop, results have also been obtained with the nacelles and fuselage camber removed for the combination with leading-edge droop.

Pressure survey.- The limited surface pressure measurements presented have been obtained in the 2-foot hypersonic facility at the Langley Research Center at a Reynolds number of 4×10^6 (based on mean aerodynamic chord) for a configuration similar to that shown in figure 6, but with 0.8° more wing incidence than that shown.

Sonic-boom measurements.- The relative magnitude of the probable sonic-boom overpressure obtainable through the use of the proposed approach has been evaluated in the Langley 4- by 4-foot supersonic pressure tunnel by using the technique described in reference 19. The several models used are shown in figure 8. The cambered swept-wing version is equivalent to the basic representative configuration shown in figure 2 except for the addition of a 4° deflection of a trailing-edge flap located near the wing-fuselage juncture. (See fig. 8.) This flap deflection provides significant improvements of the maximum lift-drag ratios at Mach numbers to about 2.0. (See ref. 9.) The aerodynamic effect of the engine nacelles on the distance field has been simulated by adding cross-sectional area equivalent to that of the nacelles along the middle and outboard regions of the wing panels. The uncambered swept-wing model has the same planform, section thicknesses, and fuselage area development as the cambered version. However, it has no wing incidence, twist, camber, dihedral, or fuselage camber. The third model simulates a typical canard delta configuration. The wing area and fuselage frontal area are the same as for the other two models. The wing thickness ratio used provides a ratio of panel span to root thickness approximately the same as that for the two highly swept configurations. The effects of nacelles for this

configuration have been simulated by adding cross-sectional area under the inboard region of the wing.

Experimental Results and Discussion

Basic aerodynamic characteristics.- The longitudinal characteristics for the basic configuration at a Mach number of 3.2 are presented in figure 9.

The probable zero-lift wave drag for the wing-nacelle part of the combination has been approximated by subtracting from the measured zero-lift drag coefficient estimated increments due to skin friction (0.0068), the fuselage nose (0.0006), fuselage camber (0.00015), nacelle toe-in (0.00015), and wing camber and twist (0.0003). This latter effect has been estimated by an extrapolation of the results obtained with the leading edge drooped and undrooped. (See fig. 10.) The estimated wave drag coefficient obtained is about 0.0007. Based on the exposed wing area, the value is 0.0009, which is approximately equal to that calculated for a 3-percent-thick delta wing with the leading edge well ahead of the Mach angle and having circular-arc airfoils.

A drag-due-to-lift factor similar to that used in previous evaluations of the effectiveness of cambered arrow wings (that is, the drag of the cambered wing at the design lift coefficient less the zero lift drag of a comparable flat wing divided by the design lift coefficient squared) has been approximated by using an estimated value of zero-lift drag for an uncambered version of the test configuration. This value has been determined by subtracting the estimated increments due to wing camber and twist and nacelle toe-in as described previously from the value measured for the cambered configuration. No adjustment for fuselage camber has been included since the increments due to this feature are roughly constant through the lift-coefficient range of interest. (See fig. 10.) A drag-due-to-lift factor of about 0.64 has been calculated for $C_L = 0.075$, which approximates the lift coefficient for the maximum full-scale lift-drag ratio. (See ref. 8.) The variation of drag with lift based on such a factor is shown by the dashed line in figure 9. This value is about 0.85 of that for a flat plate with the leading edge ahead of the Mach angle. However, it is about 1.3 times the optimum factor predicted by linear theory for a pointed-tip wing with a planform roughly equivalent to that of the experimental configuration. (A ratio of root chord to length of 0.55 was assumed for this comparable configuration.) An analysis of the nonlinear flow distortions suggests that for a given value of $\beta \cot \Lambda$ the deviations of the actual drag-due-to-lift factor from the optimum should probably be greater at higher design Mach numbers and less at lower Mach numbers.

The proposed wing fuselage combination has a zero-lift pitching-moment coefficient of about 0.008 at $M = 3.2$. (See fig. 9.) This value provides trim at a lift coefficient of 0.07 for the selected center-of-gravity location. (The results presented in references 8 and 9 indicate that this location should allow reasonable stability at most off-design flight conditions.)

The general shapes of the chordwise and spanwise pressure distributions measured on the basic configuration at a lift coefficient near that for maximum

full-scale lift drag (fig. 11) are roughly similar to the design distributions shown in figure 6.

Effect of leading-edge droop, nacelles, and fuselage camber.- The increments presented in figure 10 indicate that the leading-edge droop resulted in no perceptible change in the drag at lift coefficients near those for maximum full-scale lift-drag ratio (roughly 0.075). Apparently, the favorable effect of any reduction in boundary-layer separation resulting from this change was offset by an adverse change in the lift distribution.

An indication of the contribution of the proposed nacelle location and shaping to the attainment of the aerodynamic characteristics described is provided by the measured increments resulting from removal of the nacelles as presented in figure 10. Addition of the estimated skin-friction drag for the nacelles $\left(\Delta C_D = 0.00065\right)$ and subtraction of the probable error due to ingestion of the wing boundary layer into the inlet $\left(\Delta C_D = 0.0001\right)$ from these measured drag increments provides an indication of the effects of the nacelles on the wave drag. These adjusted values suggest that at zero lift the addition of the nacelles reduces the wave drag coefficient about 0.0009. This increment is equal to half the estimated wave drag coefficient of 0.0018 for an uncambered wing in the presence of the fuselage. At lift coefficients near that for maximum full-scale lift-drag ratio, the addition of the nacelles reduces the wave drag by about 0.0014. The additional effect at the higher lift coefficients probably results primarily from the reduction of the influence of the thickness on nonlinear effects at lifting conditions discussed earlier. It is probably also due in part to a reduction of boundary-layer separation.

In contrast to the favorable effect of the present engine installations the addition of pylon-mounted, external nacelles with no favorable intereference should result in substantial increases in the drag coefficient. It has been estimated that, at full-scale conditions, the drag-coefficient increment due to the addition of such external nacelles, comparable in size to those of the present configuration, would be approximately 0.0020 greater than those for the proposed installation.

The results presented in figure 10 indicate that fuselage camber increases the pitching-moment coefficient by 0.008 with only a small associated drag penalty.

Estimated effects of β cot Λ.- A rough indication of the effect β cot Λ on the basic drag parameters for the test configuration is provided by the results presented in figure 12. The variations shown are based on zero-lift wave-drag increments and drag-due-to-lift factors similar to those discussed for the design condition determined from experimental results for Mach numbers of 2.6, 2.96, 3.2, and 3.5. (See ref. 8.) The values of β cot Λ corresponding to these Mach numbers are 0.66, 0.77, 0.84, and 0.93. The first-order effects of Mach number have been removed from the variations by multiplying the zero-lift wave-drag increments by β and dividing the drag-due-to-lift factors by this term.

The results indicate that the zero-lift wave-drag factor is roughly constant with an increase in $\beta \cot \Lambda$ to about 0.84 but rises abruptly with an increase of $\beta \cot \Lambda$ to 0.93. This change probably results from a convergence of positive disturbances near the leading edge of the wing for this condition. The adjusted drag-due-to-lift factor is approximately constant with an increase in $\beta \cot \Lambda$ to 0.93.

Sonic boom.- An indication of the relative intensity of the sonic-boom overpressure for the proposed configurations for a Mach number of 2.0 is provided by the results presented in figure 13. These values have been estimated on the basis of the measured overpressures by using the procedure described in reference 19. The measurements used were obtained at a distance of 43.5 fuselage lengths from the test model. Surveys at this distance usually provide a fairly reliable indication of far-field conditions. Also, the results shown have been corrected, by using the theory of reference 18, for the effect of laminar boundary-layer growth on the models. The magnitudes of these adjustments are indicated in figure 13. The results have been made nondimensional in terms of distance in the usual manner. (See ref. 19.) A length of 1.15 inches has been assumed for all the models investigated.

At Mach numbers near 2.0, a supersonic transport will probably climb at lift coefficients near 0.15. For such conditions the boom intensity for the proposed configuration is about 0.7 of that for the comparable delta airplane. The difference is due to both a lower pressure at zero lift and a reduced increment due to lift for the swept-wing version.

In order to provide an indication of the influence of nonlinear effects on the magnitude of the sonic boom for the experimental configurations, maximum pressures predicted by using the linear theory are also shown in figure 13. In the computations for the lifting conditions, the lift was assumed to be distributed uniformly on the wing and canard of the delta configuration. For the swept configuration, an elliptic longitudinal distribution along the length of the exposed wing was assumed. The distributions were extended longitudinally to account for the dihedral. At a lift coefficient of zero, a distribution of lift which provides the pitching-moment coefficient measured for this condition (ref. 8) was used. Although the experimental maximum pressures for the canard delta are somewhat greater than predicted, the measured values for the swept configuration are significantly less. The measured overpressures are roughly equal to the minimum values described in reference 20 for the lift-coefficient range of interest.

The experimental boom pressure for the cambered configuration is of the same order as that for the uncambered model for lift coefficients near 0.15 (fig. 13), even though the longitudinal lift distribution on the uncambered configuration is significantly more favorable from the standpoint of boom intensity. It appears that this adverse effect of the loading distribution on the cambered wing is offset by the favorable effect of the dihedral built into this model that was discussed earlier.

CONCLUDING REMARKS

An analysis of the results presented herein for a wing-nacelle-fuselage combination based on the proposed design approach suggests that the possible supersonic lift-drag ratios for an actual airplane based on this method should be significantly higher than those for a comparable delta-wing configuration at least for Mach numbers to 3.2. The results presented indicate the most important factor contributing to the improved supersonic drag characteristics is the special placement of the engine nacelles along the rearward part of the wing. The gain is also due in part to the low ratio of root chord to wing length and a reduced trim penalty.

The measured sonic-boom overpressures for the suggested configuration are not only substantially less than those for a comparable delta-wing configuration but also approach the minimum level indicated by linear theory. The increased aspect ratios provided by the low ratio of root chord to wing length and reduced sweep angles of the proposed approach should allow reasonable lift-drag ratios at lower speeds. With the increased wing-section thickness ratios utilized and the favorable weight distributions allowed by the special placement of the engine nacelles, the wing structural weight for an airplane based on the proposed configuration should not be excessive.

Langley Research Center,
National Aeronautics and Space Administration,
Langley Station, Hampton, Va., December 14, 1962.

APPENDIX A

AREA-RULE ANALYSES

Longitudinal Area Developments

The fundamental justification for the use of longitudinal developments of cross-sectional area to define the zero-lift wave-drag problem is not nearly as strong for the higher supersonic Mach numbers as at lower speeds. However, several comparisons have indicated that, when the proper developments are used, reasonably good agreement between area-rule predictions and measurements can be obtained at these higher speeds for arrow-wing configurations with the leading edge swept behind the Mach angle.

The basic methods used are similar to those described in reference 22. Because of the extreme obliqueness of the cutting planes at these higher Mach numbers, many of the simplifying assumptions of reference 22 used in determining cross-sectional areas for the lower speed cases cannot be justified. The actual cross-sectional areas intersected by the cutting planes must be used.

The requirement that the area developments for above and below the wing chord plane be considered separately as discussed in reference 22 is even more important at the higher Mach numbers than at lower speeds. For the present configuration with dihedral, the areas have been divided by two oblique planes which pass through the leading edge of the wing panels and are parallel to the streamwise reference axis. To reduce to a minimum the effects of the unpredictable vertical flows ahead of the wing leading edge, the area analysis of figure 4 has been made for an angle of attack at which the mean wing surface near the leading edge is roughly alined with the streamwise reference axis.

To account partially for the flow nonlinearities, the area developments for the upper surface have been obtained with cuts corresponding to a Mach number of 3.3, those for the lower surface with cuts for $M = 3.0$, rather than the nominal Mach number of 3.2.

Effective Surface Shapes

As suggested in reference 12, the combined effects of the upper or lower parts of the wing and nacelles on the effective field above or below the wing should be similar to that for an equivalent wing with the cross-sectional area of the nacelles above or below the wing distributed along the local wing upper or lower surface. As indicated in reference 12, the most valid equivalent wing surfaces are probably obtained with the nacelle areas determined by cuts parellel to constant percent chord lines and then distributed along these same lines. The effective mean surface for the combination should be roughly the mean between the equivalent surfaces for the upper and lower parts.

APPENDIX B

WING STRUCTURAL CONSIDERATIONS

Flutter

Results of pertinent experiments indicate that flutter should probably not be a controlling factor in defining the wing stiffness. The data of reference 23 indicate that the flutter q values for wings with sweeps similar to that of the present configuration are much greater than those for comparable wings with less sweep. Further, results presented in reference 24 indicate that the placement of engine masses near the trailing edge of a wing panel similar to that of the present configuration resulted in an increase of flutter q at the critical high subsonic and transonic speed conditions. This effect, which is opposite to that which might be expected on the basis of previous experience, can be predicted by using a logical extension of present flutter theory. (See ref. 25.)

Bending Moments

The outboard locations of the engine nacelles, of course, reduces the maximum bending moments acting at the inboard sections of the wing, as for many present subsonic airplanes. For the highly swept wing of the present approach, this effect is enhanced by the proposed rearward displacement of the engines. An abbreviated design analysis of a representative transport airplane based on the proposed approach suggests that the downward bending moments produced at the structurally critical region by the weight of the outboard components should be almost half the upward moment resulting from aerodynamic loads at the fully loaded, level-flight condition. With this favorable factor and the relatively thick wing sections used, the weight of the wing structure required to withstand bending moments should be of reasonably small magnitude.

REFERENCES

1. Patton, R. J.: Supersonic Transport Design Characteristics and the Sonic Boom. Paper No. 62-23, Inst. Aerospace Sci., Jan. 1962.

2. Jones, Robert T.: Estimated Lift-Drag Ratios at Supersonic Speed. NACA TN 1350, 1947.

3. Brown, Clinton E., and McLean, Francis E.: The Problem of Obtaining High Lift-Drag Ratios at Supersonic Speeds. Jour. Aero/Space Sci., vol. 26, no. 5, May 1959, pp. 298-302.

4. Hallissy, Joseph M., Jr., and Hasson, Dennis F.: Aerodynamic Characteristics at Mach Numbers 2.36 and 2.87 of an Airplane Configuration Having a Cambered Arrow Wing With a 75° Swept Leading Edge. NACA RM L58E21, 1958.

5. Carlson, Harry W.: Aerodynamic Characteristics at Mach Number 2.05 of a Series of Highly Swept Arrow Wings Employing Various Degrees of Twist and Camber. NASA TM X-332, 1960.

6. Hasson, Dennis F., Fichter, Ann B., and Wong, Norman: Aerodynamic Characteristics at Mach Numbers from 1.6 to 2.8 of 74° Swept Arrow Wings With and Without Camber and Twist. NASA TM X-8, 1959.

7. Hasson, Dennis F., and Wong, Norman: Aerodynamic Characteristics at Mach Numbers From 2.29 to 4.65 of 80° Swept Arrow Wings With and Without Camber and Twist. NASA TM X-175, 1960.

8. Whitcomb, Richard T., Patterson, James C., Jr., and Kelly, Thomas C.: An Investigation of the Subsonic, Transonic, and Supersonic Aerodynamic Characteristics of a Proposed Arrow-Wing Transport Airplane Configuration. NASA TM X-800, 1963.

9. Whitcomb, Richard T., and Loving, Donald L.: An Investigation of the Landing and Take-Off Characteristics of a Proposed Arrow-Wing Transport Airplane Configuration. NASA TM X-801, 1963.

10. Carlson, Harry W.: Pressure Distributions at Mach Number 2.05 on a Series of Highly Swept Arrow Wings Employing Various Degrees of Twist and Camber. NASA TN D-1264, 1962.

11. Whitcomb, Richard T.: Special Bodies Added on a Wing to Reduce Shock-Induced Boundary-Layer Separation at High Subsonic Speeds. NACA TN 4293, 1958.

12. Loving, Donald L.: A Wind-Tunnel Investigation of a Transonic-Transport Configuration Utilizing Drag-Reducing Devices at Mach Numbers From 0.20 to 1.03. NASA TN D-636, 1961.

13. Spearman, M. Leroy, and Driver, Cornelius: Some Factors Affecting the Stability and Performance Characteristics of Canard Aircraft Configurations. NACA RM L58D16, 1958.

14. Whitcomb, Richard T.: A Fuselage Addition to Increase Drag-Rise Mach Number of Subsonic Airplanes at Lifting Conditions. NACA TN 4290, 1958.

15. Donovan, A. F., and Lawrence, H. R., eds.: Aerodynamic Components of Aircraft at High Speeds. Vol. VII of High Speed Aerodynamics and Jet Propulsion, Princeton Univ. Press, 1957.

16. Hasson, Dennis F., Fichter, Ann B., and Wong, Norman: Pressure Distributions at Mach Numbers From 1.6 to 2.8 of 74° Swept Arrows Wings With and Without Camber and Twist. NASA TM X-190, 1960.

17. O'Hara, F., and Scott-Wilson, J. B.: An Investigation of the Flow Over a Half-Wing Model With 60.5 Degrees Leading Edge Sweepback, at a High Subsonic and Supersonic Speeds. Rep. No. AERO 2567, British R.A.E., Nov. 1955.

18. Walkden, F.: The Shock Pattern of a Wing-Body Combination, Far From the Flight Path. Aero. Quarterly, vol. IX, p. 2, May 1958, pp. 164-194.

19. Carlson, Harry W.: Wind-Tunnel Measurements of the Sonic-Boom Characteristics of a Supersonic Bomber Model and a Correlation With Flight-Test Ground Measurements. NASA TM X-700, 1962.

20. Carlson, Harry W.: The Lower Bound of Attainable Sonic-Boom Overpressure and Design Methods of Approaching This Limit. NASA TN D-1494, 1962.

21. Conners, James F., and Anderson, Leverett A., Jr.: A Two-Dimensional External-Internal-Compression Inlet With Throat Bypass at Mach 3.05. NASA MEMO 10-3-58E, 1958.

22. Whitcomb, Richard T.: Some Considerations Regarding the Application of the Supersonic Area Rule to the Design of Airplane Fuselages. NACA RM L56E23a, 1956.

23. Stonesifer, John C., and Goetz, Robert C.: Transonic and Supersonic Flutter Trend Investigation of a Variable-Sweep Wing. NASA TM X-598, 1961.

24. Walberg, Gerald D.: Transonic Flutter Tests of a Highly Swept Arrow Wing With and Without Simulated Trailing-Edge-Mounted Engine Masses. NASA TN D-1023, 1962.

25. Walberg, Gerald D.: Investigation of the Subsonic Flutter Characteristics of a Highly Swept Arrow Planform Wing With and Without Simulated Trailing-Edge-Mounted Engine Masses. M.S. Thesis, Virginia Polytechnic Institute, 1962.

TABLE I

DESCRIPTION OF EXPERIMENTAL CONFIGURATION

(a) Wing dimensions

Sweep, deg	74.5
Aspect ratio	1.72
Taper ratio	0.15
Root chord/Length	0.53
Area, sq ft	1.43
Mean aerodynamic chord, ft	1.08
Span, ft	1.57
Airfoil section	Modified circular arc
Thickness-chord ratio (mean)	0.05
Twist (overall), deg:	
Drooped leading edge	2.8
Undrooped leading edge	1.9
Incidence (mean) (leading edge drooped), deg	1.5
Dihedral (mean), deg	19

TABLE I.- Continued

DESCRIPTION OF EXPERIMENTAL CONFIGURATION

(b) Airfoil coordinates

Distance from leading edge, x', in.	Airfoil coordinates for - Drooped leading edge	
	y_u, in.	y_l, in.
Span station, 1.80 in.		
0	0	0
.2	.075	-.065
.5	.110	-.105
1.0	.130	-.165
2.0	.160	-.270
3.0	.165	-.380
4.0	.165	-.485
5.0	.155	-.580
6.0	.130	-.665
7.0	.095	-.750
8.0	.060	-.815
9.0	-.005	-.860
10.0	-.075	-.895
11.0	-.155	-.895
12.0	-.245	-.895
13.0	-.325	-.880
14.0	-.410	-.845
15.0	-.495	-.815
16.0	-.595	-.740
16.70	-.670	-.670
Span station, 3.04 in.		
0	0	0
.2	.075	-.065
.5	.105	-.100
1.0	.140	-.160
2.0	.170	-.265
3.0	.185	-.370
4.0	.185	-.460
5.0	.160	-.535
6.0	.135	-.605
7.0	.080	-.640
8.0	.025	-.660
9.0	-.065	-.660
10.0	-.165	-.640
11.0	-.290	-.615
12.0	-.420	-.570
12.65	-.510	-.510
Span station, 4.23 in.		
0	0	0
.2	.085	-.070
.5	.120	-.115
1.0	.155	-.980
2.0	.200	-.975
3.0	.225	-.950
4.0	.240	-.945
5.0	.255	-.955
6.0	.270	-.960
7.0	.290	-.980
8.0	.305	-.995
9.0	.320	-1.000
10.0	.335	-1.010
10.81	.340	1.040

TABLE I.- Continued

DESCRIPTION OF EXPERIMENTAL CONFIGURATION

(b) Airfoil coordinates - Concluded

Distance from leading edge, x', in.	Airfoil coordinates for -			
	Drooped leading edge		Undrooped leading edge	
	y_u, in.	y_l, in.	y_u, in.	y_l, in.
Span station, 5.42 in.				
0	0	0	0.042	0.042
.2	.060	-.070	.115	-.010
.5	.090	-.095	.150	-.050
1.0	.120	-.140	.185	-.090
2.0	.160	-.205	.220	-.170
3.0	.175	-.260	.220	-.240
4.0	.180	-.295	.195	-.285
5.0	.150	-.305	.150	-.305
6.0	.085	-.300	.085	-.300
7.0	.010	-.275	.010	-.275
8.0	-.070	-.230	-.070	-.230
9.0	-.145	-.170	-.145	-.170
9.025	-.150	-.150	-.150	-.150
Span station, 6.60 in.				
0	0	0	0.052	0.052
.2	.095	-.055	.135	-.015
.5	.135	-.085	.170	-.045
1.0	.180	-.740	.210	-.740
2.0	.240	-.880	.260	-.860
3.0	.295	-.850	.310	-.850
4.0	.340	-.830	.355	-.830
5.0	.390	-.820	.405	-.820
6.0	.450	-.810	.450	-.810
7.0	.495	-.800	.495	-.800
7.45	.520	-.800	.520	-.800
Span station, 7.80 in.				
0	0	0	0.061	0.061
.2	.055	-.055	.105	-.005
.5	.095	-.075	.135	-.045
1.0	.135	-.085	.160	-.075
2.0	.190	-.095	.190	-.095
3.0	.190	-.090	.190	-.090
4.0	.160	-.060	.160	-.060
5.0	.100	-.020	.100	-.020
5.9	.030	.030	.030	.030
Span station, 8.98 in.				
0	0	0	0.070	0.070
.2	.075	-.045	.125	.000
.5	.115	-.060	.140	-.005
1.0	.155	-.050	.160	-.030
2.0	.160	-.025	.160	-.025
3.0	.125	.000	.125	.000
4.0	.075	.020	.075	.020
4.42	.050	.050	.050	.050

TABLE I.- Concluded

DESCRIPTION OF EXPERIMENTAL CONFIGURATION

(c) Fuselage coordinates

Distance from nose, in.	Fuselage coordinates, in., for -		
	Upper surface	Lower surface	Sides (from center line)
0.25	0	-0.06	0.02
11	.88	-1.12	.99
11.5	.92	-1.17	1.03
12	.96	-1.21	1.08
12.5	.98	-1.27	1.12
13	.99	-1.32	1.16
13.5	.98	-1.37	1.19
14	.95	-1.43	1.22
15	.87	-1.52	1.24
16	.78	-1.63	1.25
17	.69	-1.73	1.25
18	.61	-1.81	1.25
19	.53	-1.88	1.25
20	.47	-1.94	1.25
21	.42	-1.99	1.25
22	.38	-2.05	1.25
23	.34	-2.11	1.25
24	.31	-2.15	1.25
25	.29	-2.19	1.25
26	.28	-2.20	1.25
27	.27	-2.21	1.25
28	.26	-2.22	1.25
29	.26	-2.22	1.24
30	.25	-2.21	1.23
31	.25	-2.17	1.22
32	.25	-2.14	1.21
33	.25	-2.10	1.19
34	.25	-2.07	1.14
35	.25	-2.02	1.11
45.75	.25	-1.45	.85

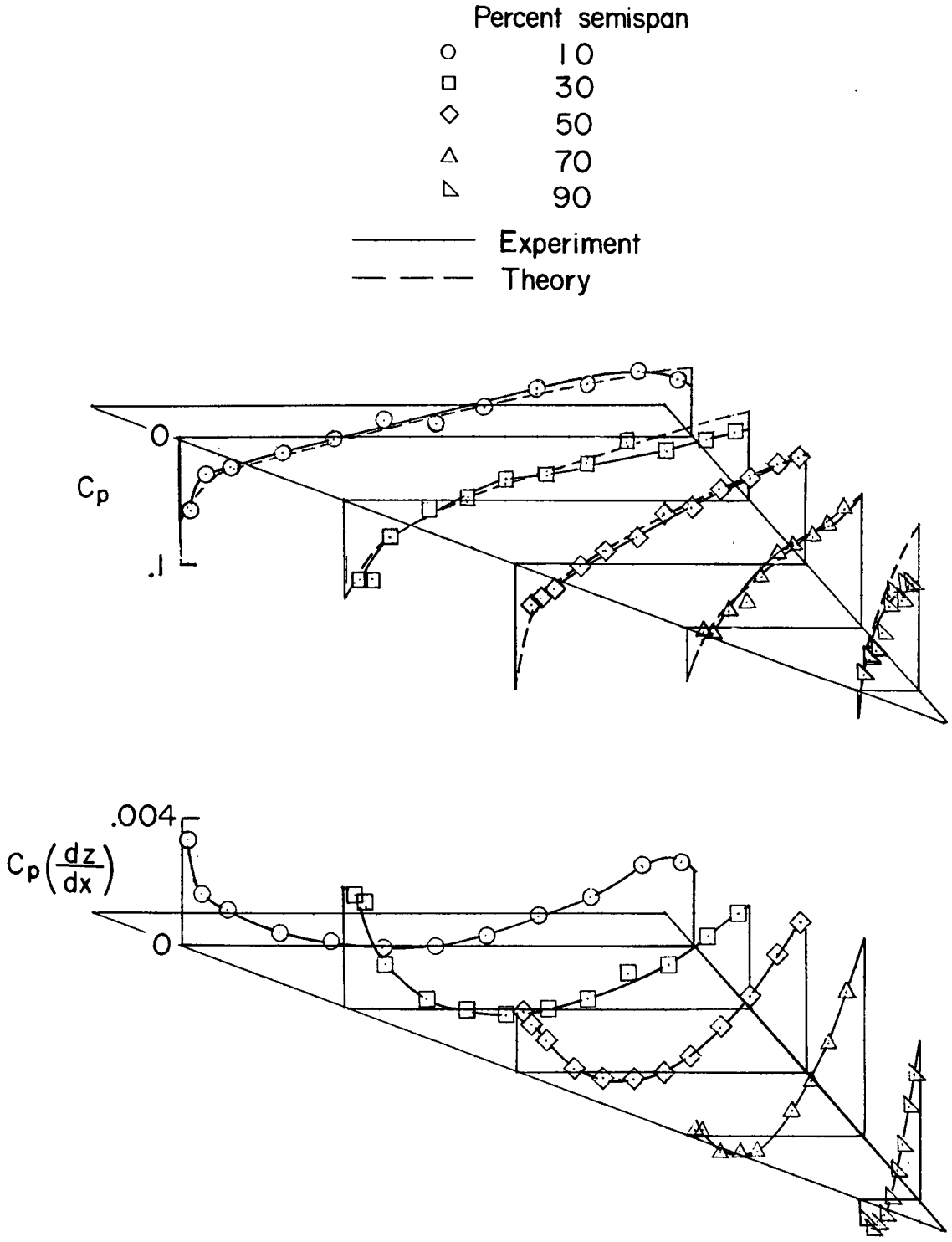

Figure 1.- Pressure and axial-force distributions on arrow wing having 70° of leading-edge sweep and t/c = 0.03 at M = 2.0 and α = 0°.

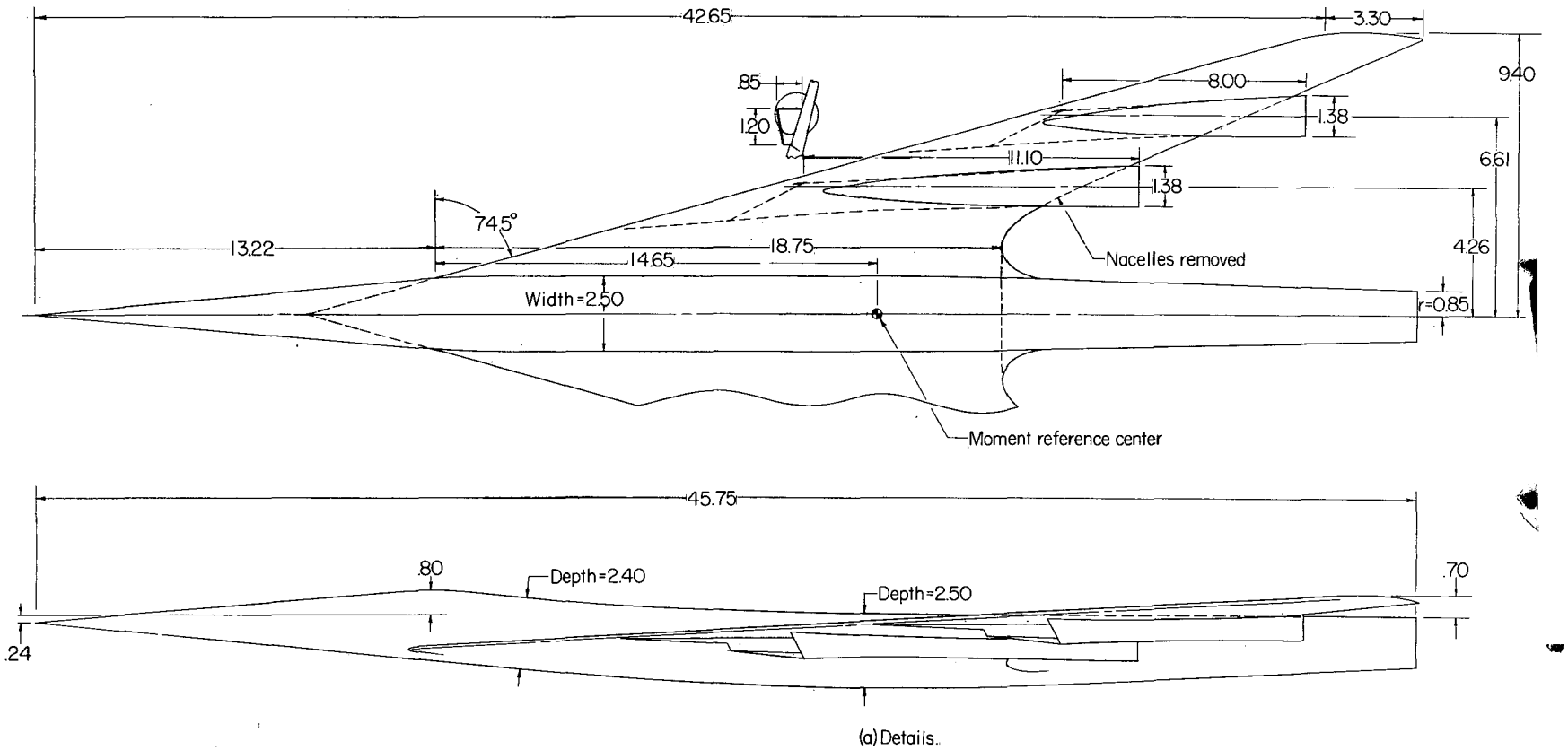

(a) Details.

Figure 2.- Description of representative configuration investigated. All dimensions are in inches unless otherwise stated.

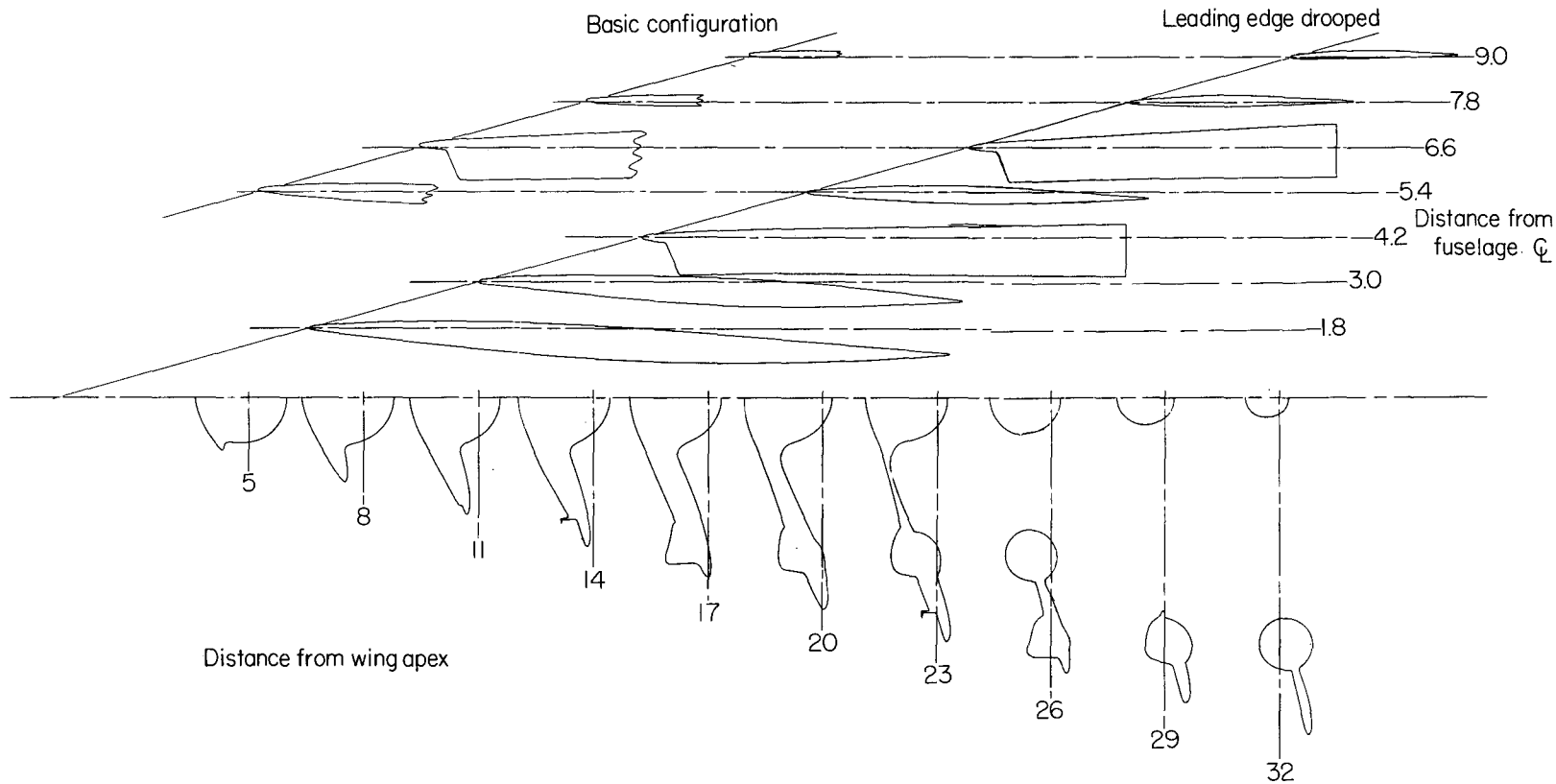

(b) Cross sections.

Figure 2.- Continued.

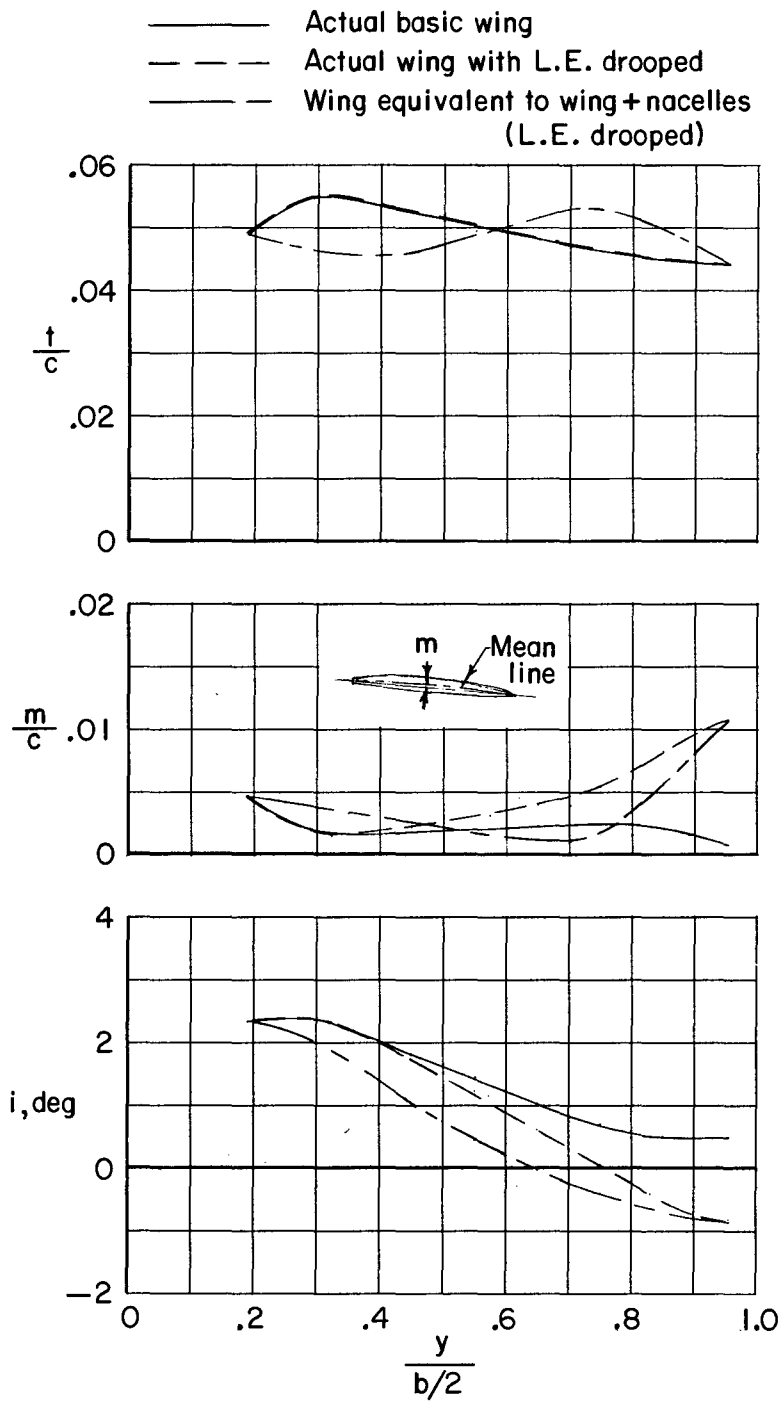

(c) Spanwise variations of local thickness ratio, maximum camber, and incidence for actual and equivalent wings.

Figure 2.- Continued.

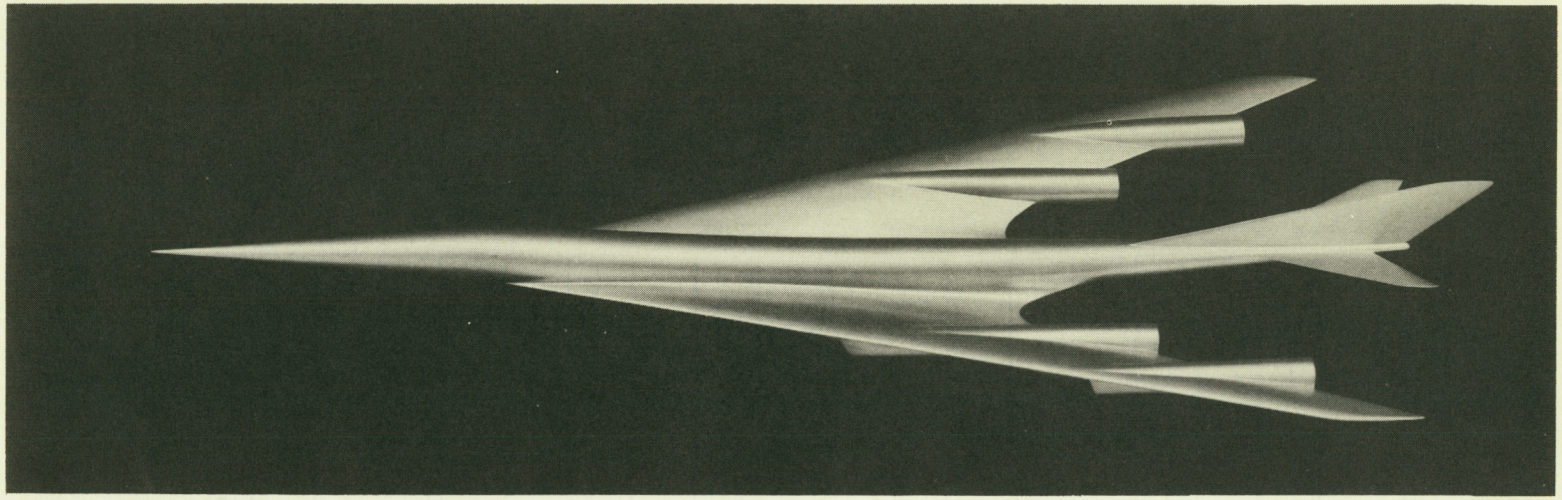

L-62-6137

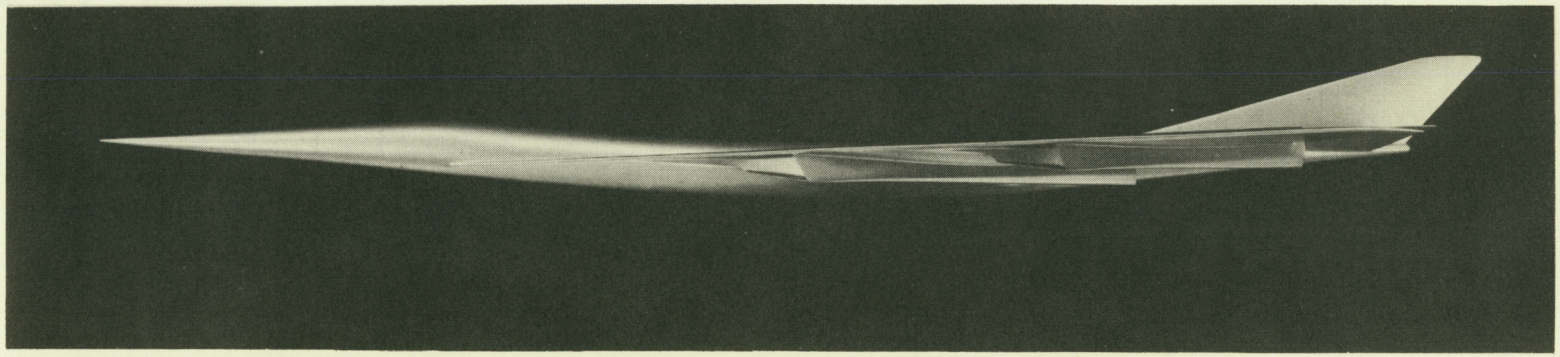

L-62-6136

(d) Three-quarter and side view of complete airplane configuration based on proposed wing-fuselage-nacelle combination.

Figure 2.- Concluded.

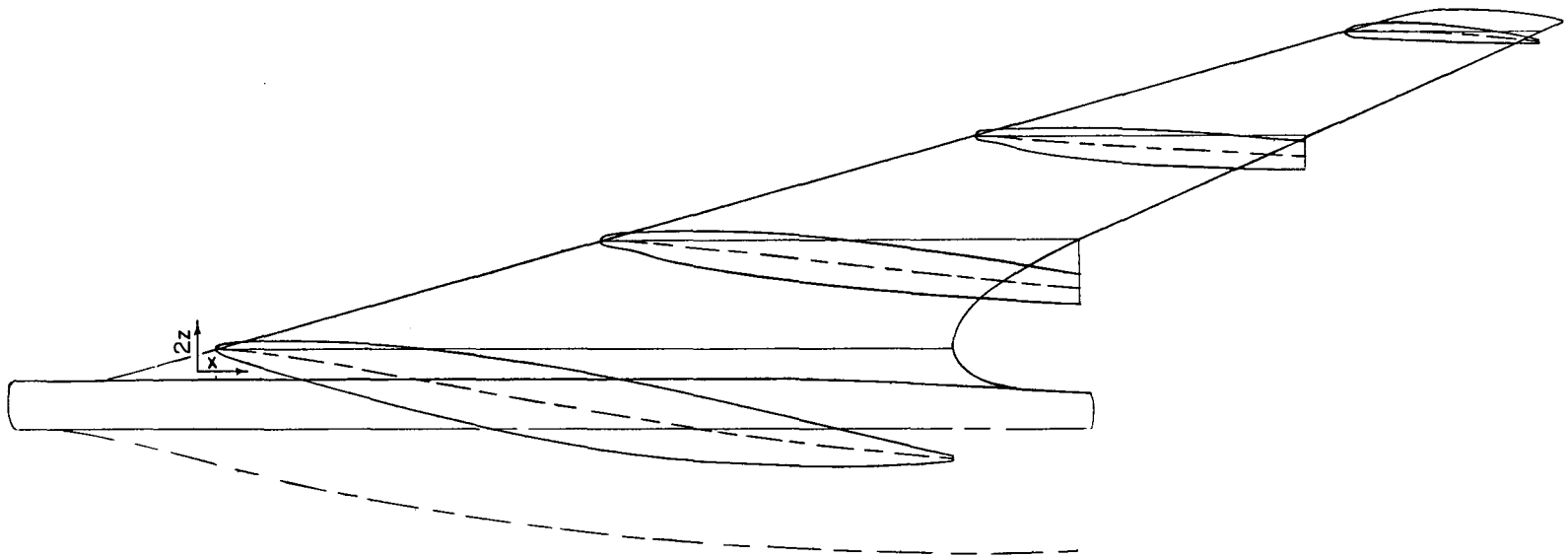

Figure 3.- Section and mean-line shapes for wing equivalent to complete representative configuration. $\alpha = 2.0^{\circ}$.

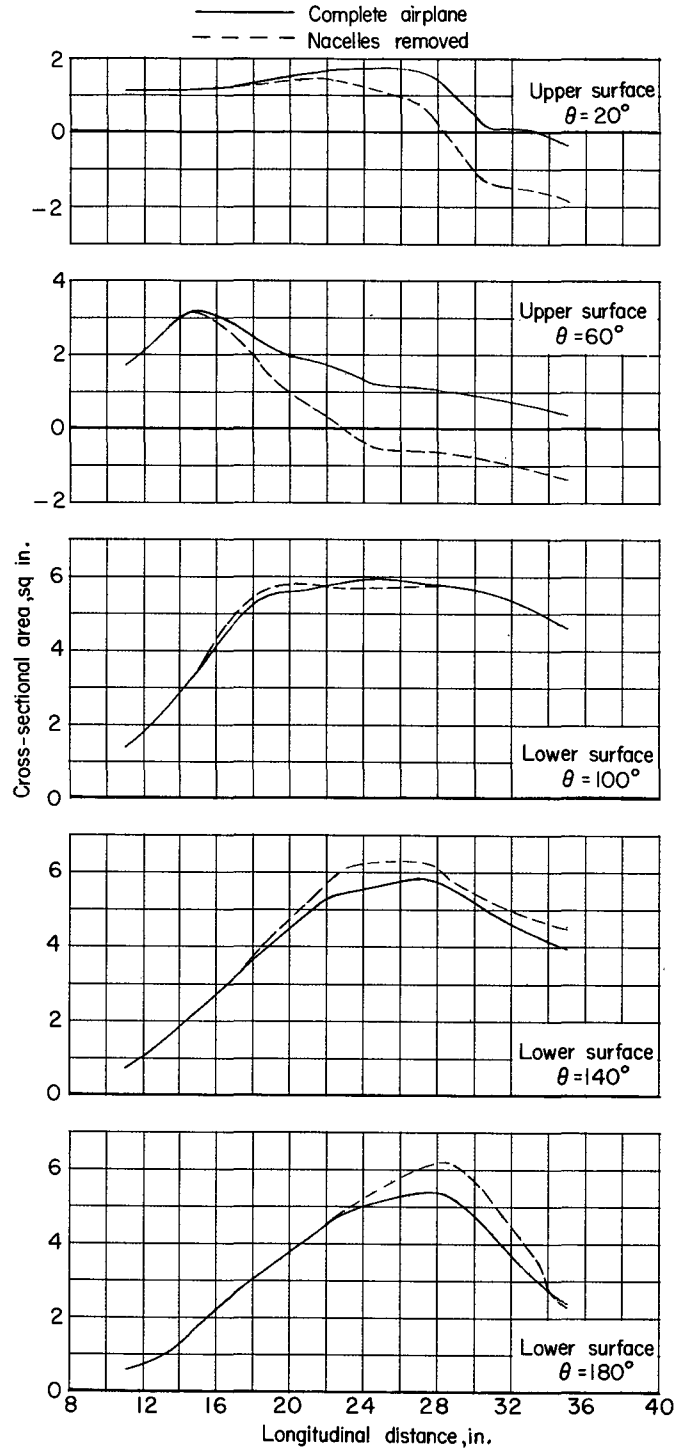

Figure 4.- Longitudinal developments of cross-sectional area for representative configuration at M = 3.2 and $\alpha = -0.6^{\circ}$.

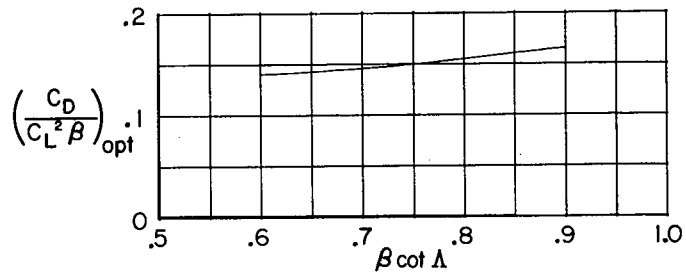

(a) Theoretically optimum drag due to lift. $c_r/l = 0.55$.

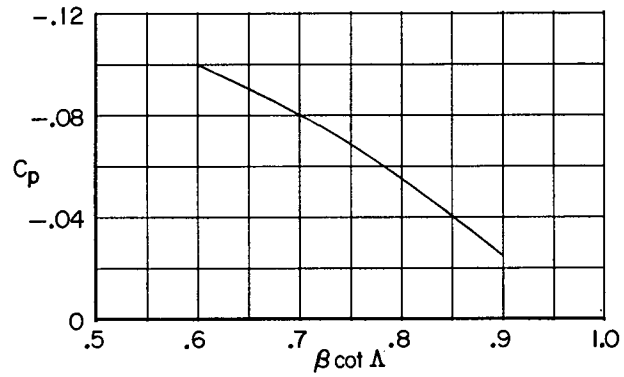

(b) Estimated pressure coefficients near the leading edge of the upper surface for theoretically optimum load distribution. $c_r/l = 0.55$; 0.70 semispan; M = 3.20; and $C_L = 0.075$.

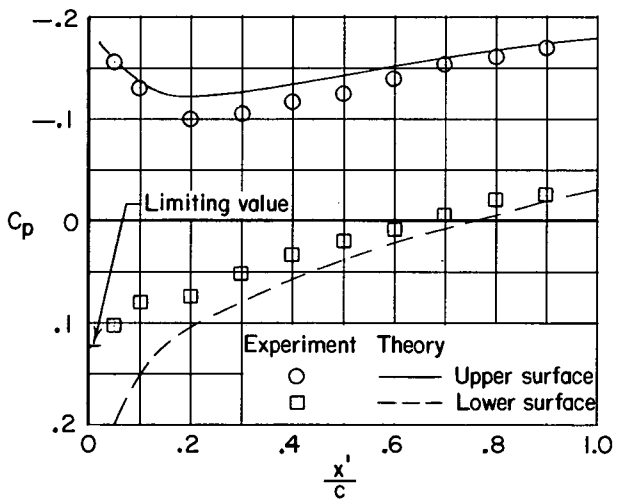

(c) Comparison of measured and theoretical pressure distributions on the 0.7-semispan-station twisted and cambered wing with 70° sweep at M = 2.0.

Figure 5.- Analysis of effects of β cot Λ.

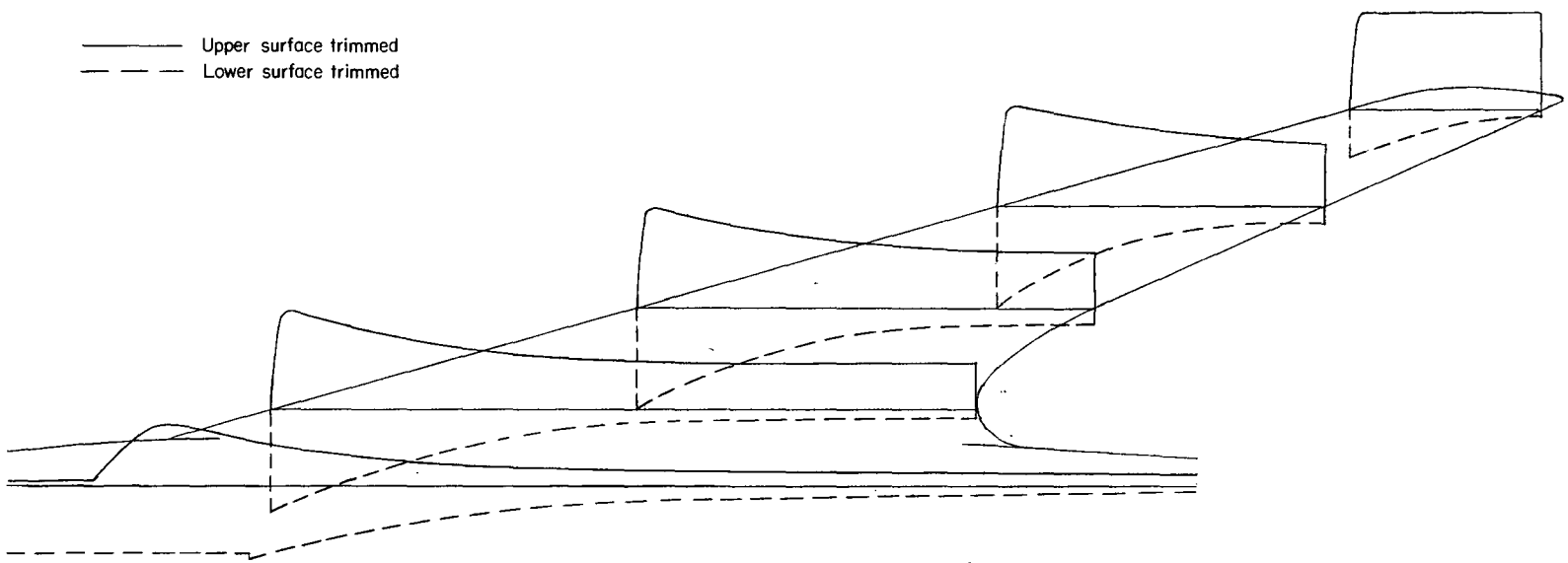

Figure 6.- Design pressure distributions for proposed configuration.

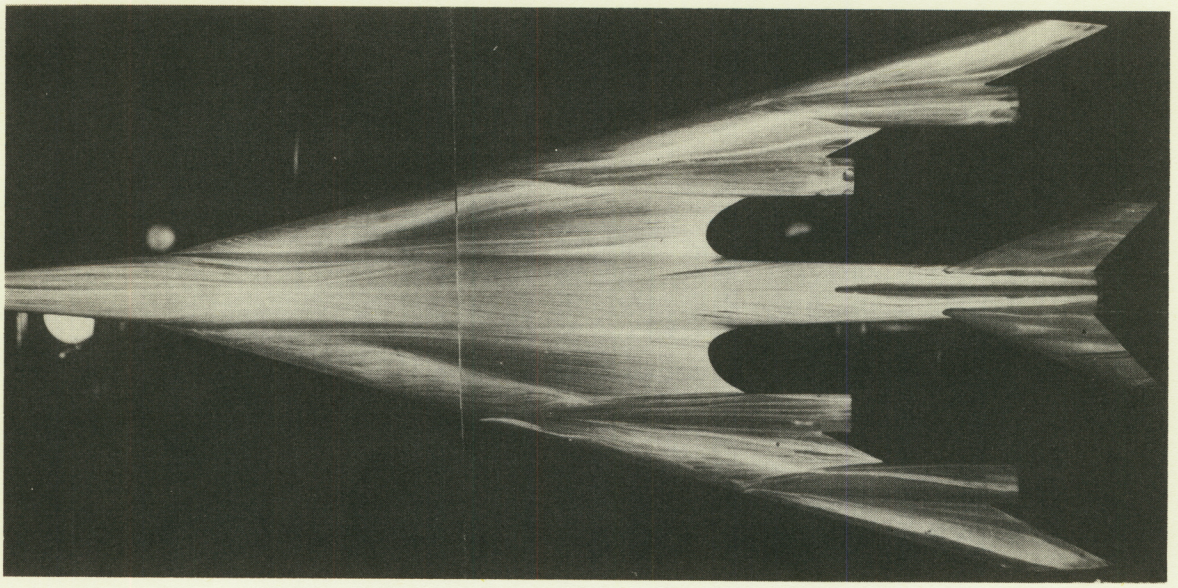

Upper surface

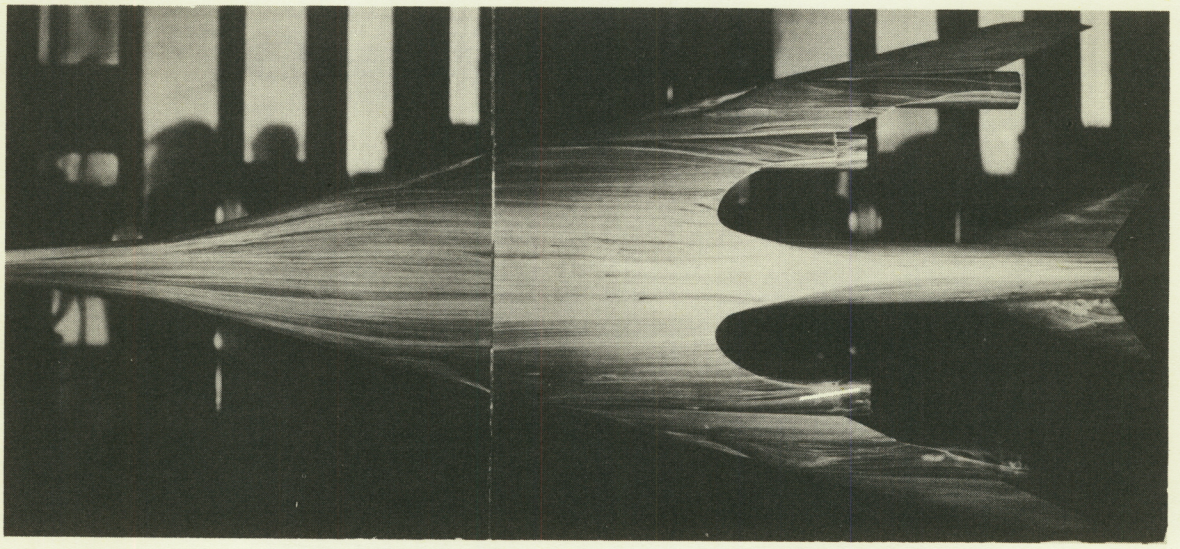

Lower surface

L-62-7063

Figure 7.- Surface oil-flow surveys on basic representative configuration at $M = 2.96$ and $C_L = 0.07$.

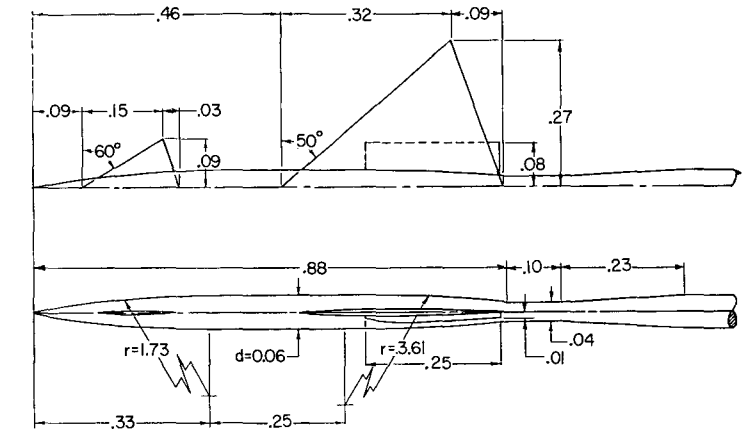

Delta-wing configuration

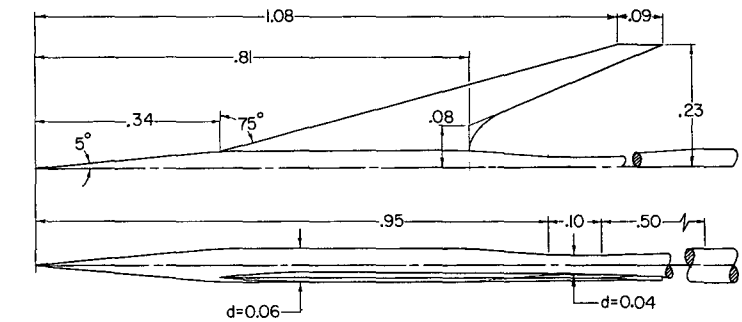

Uncambered swept-wing configuration

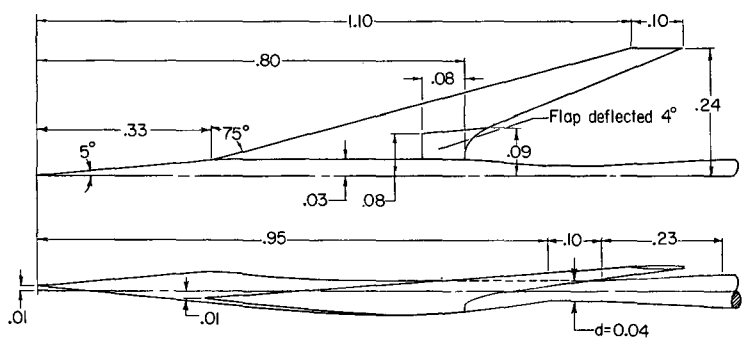

Cambered swept-wing configuration

(a) Details. All dimensions are in inches unless otherwise noted.

Figure 8.- Models used in investigation of sonic boom for representative configuration.

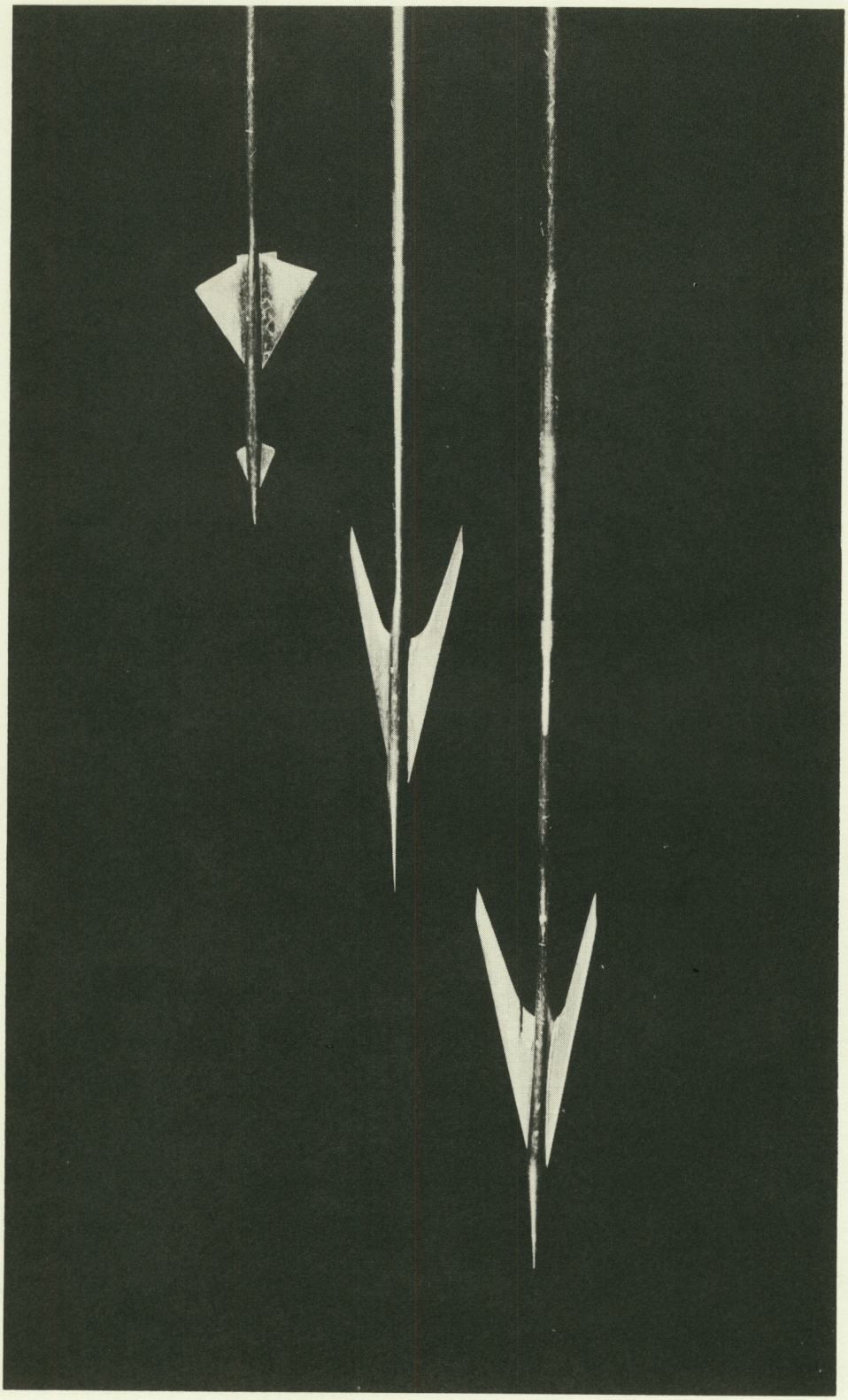

(b) Three-quarter views of models. L-62-6169

Figure 8.- Concluded.

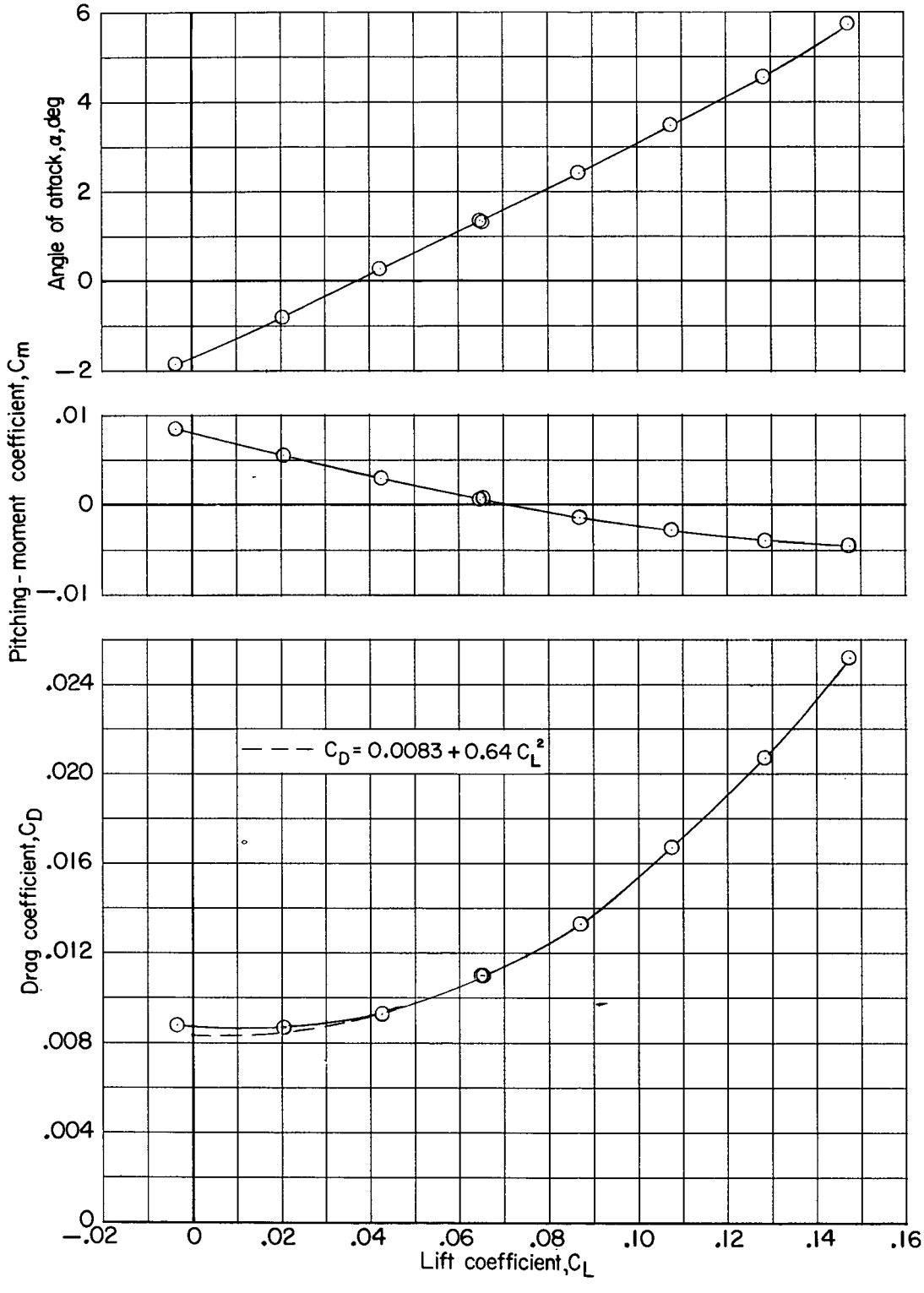

Figure 9.- Longitudinal aerodynamic characteristics of basic representative configuration at M = 3.2.

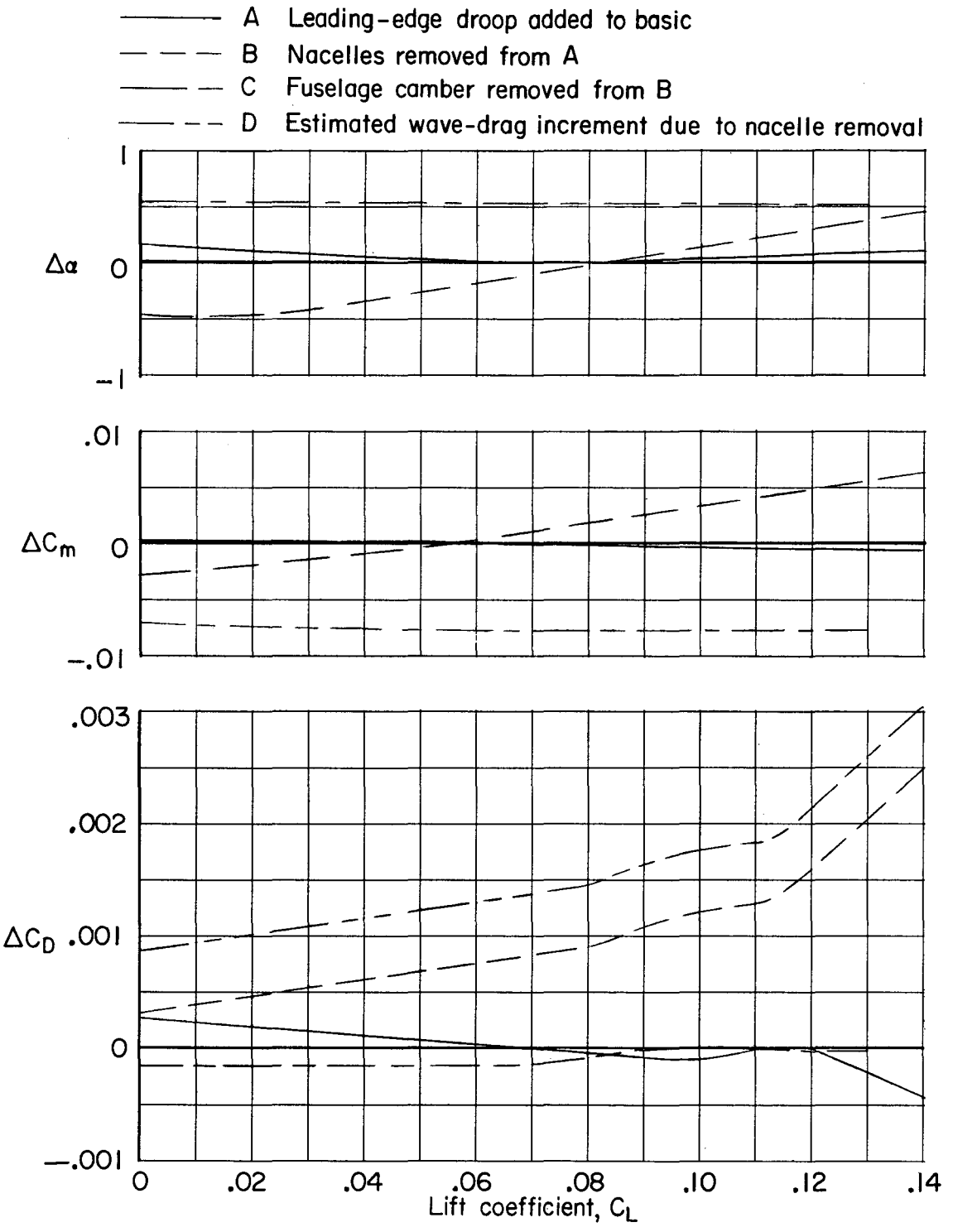

Figure 10.- Increments in longitudinal characteristics due to addition of leading-edge droop, removal of nacelles, and removal of fuselage camber at M = 3.2.

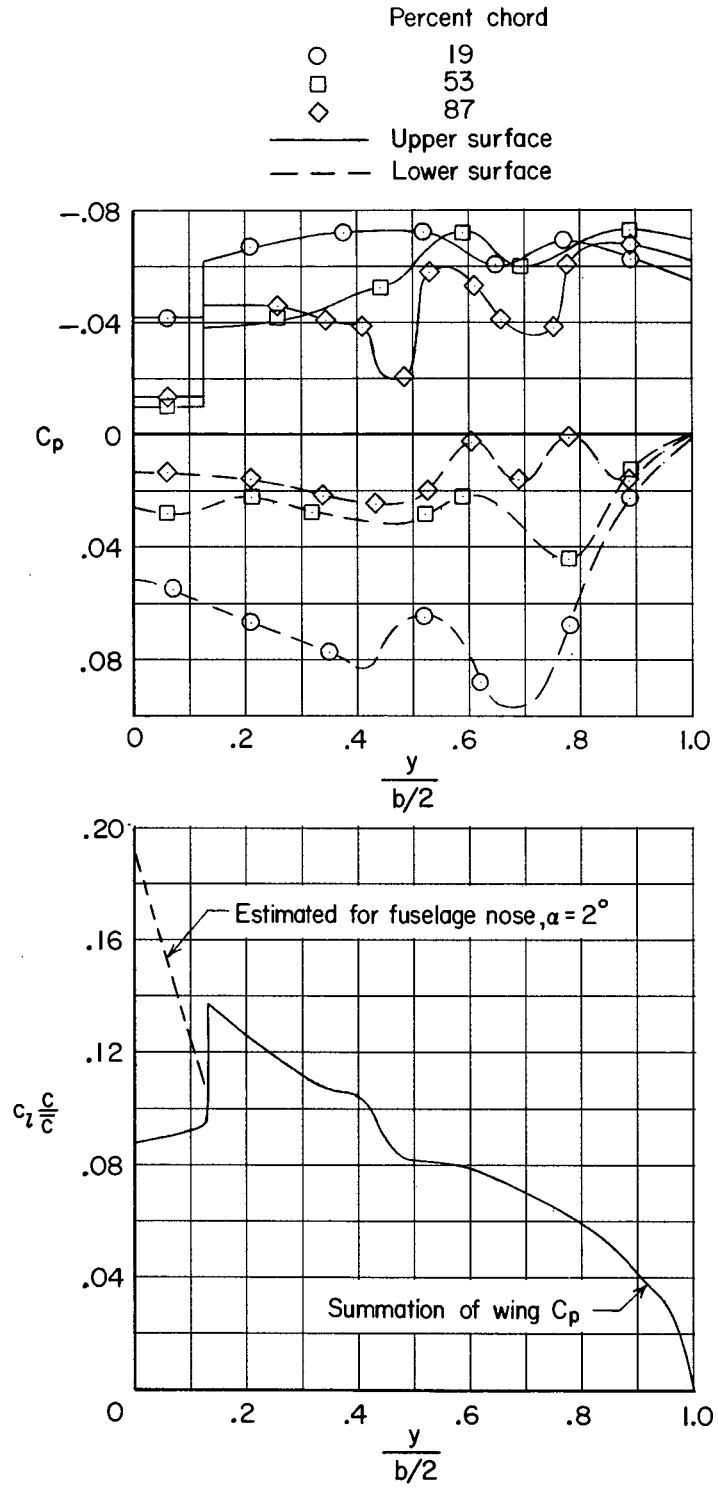

Figure 11.- Measured pressure and span-load distributions for model approximating representative configuration at $C_L = 0.08$ and $M = 3.2$.

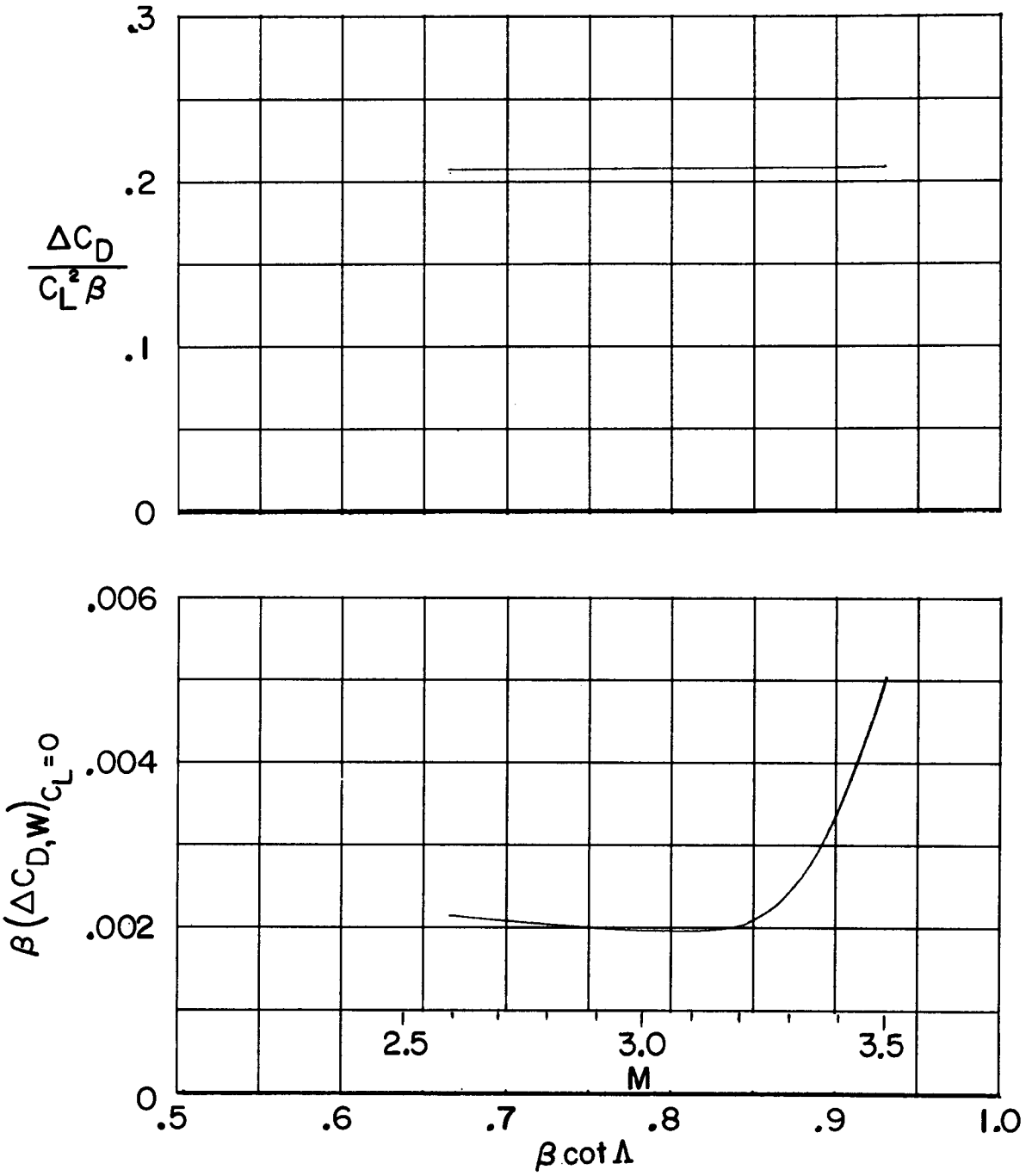

Figure 12.- Estimated variations with $\beta \cot \Lambda$ of the estimated zero-lift wave-drag increment for uncambered wing nacelle combination similar to the experimental configuration and the drag-due-to-lift factor for the experimental configuration.

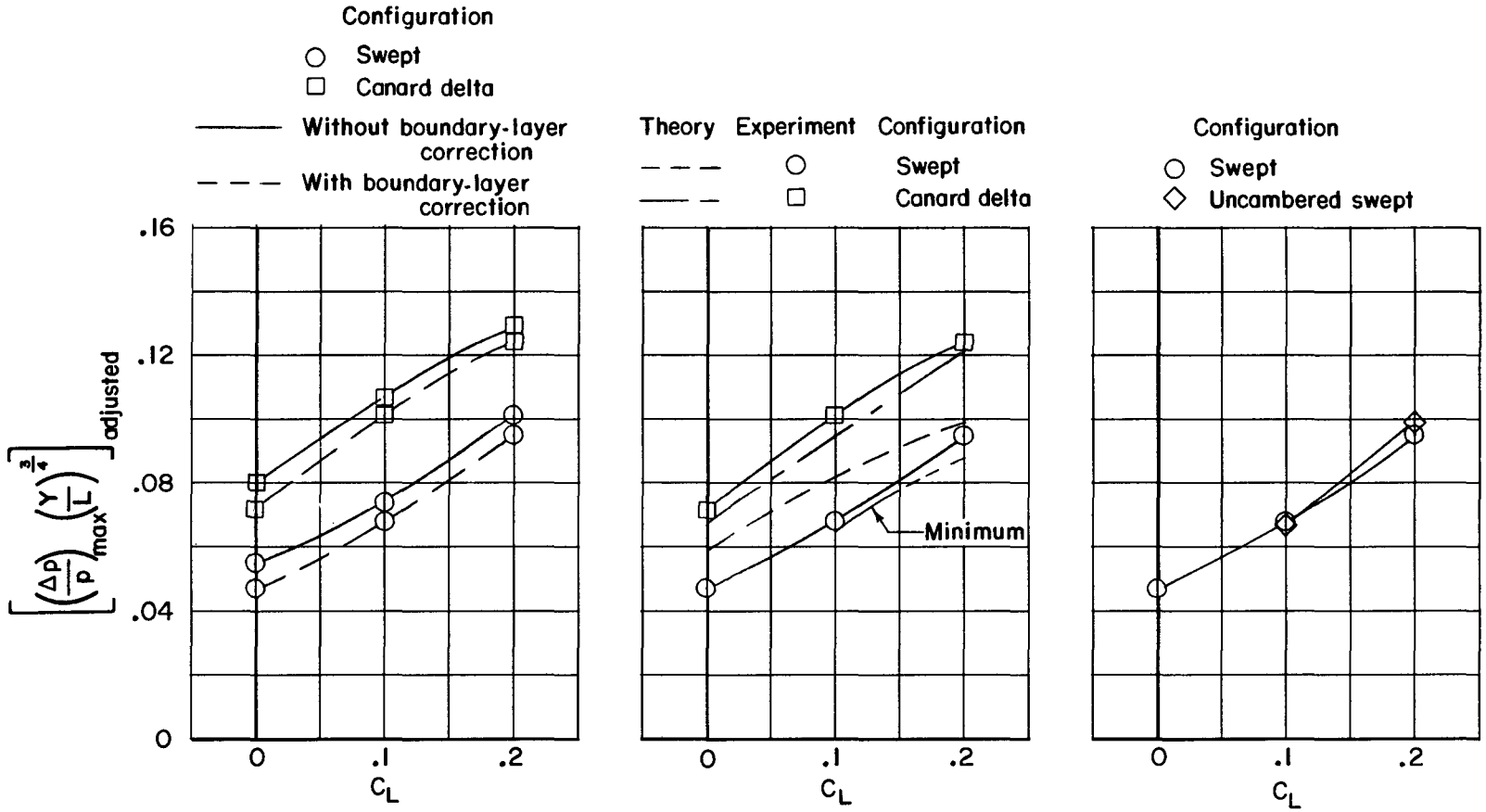

Figure 13.- Variations of maximum sonic-boom pressure with lift coefficient for several configurations at M = 2.01 y/L = 43.5.